

ANALYSIS OF A WIRE ANTENNA BY SOLVING  
POCKLINGTON'S INTEGRAL EQUATION USING WAVELETS

BY

BINDUBRITTA ACHARJEE

A THESIS

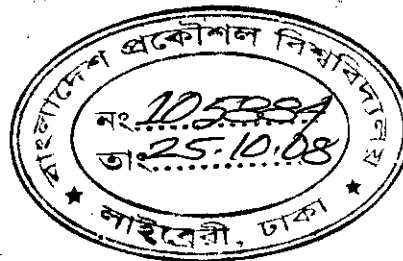
SUBMITTED TO THE DEPARTMENT OF ELECTRICAL AND ELECTRONIC  
ENGINEERING

IN PARTIAL FULFILLMENT OF THE REQUIREMENTS FOR

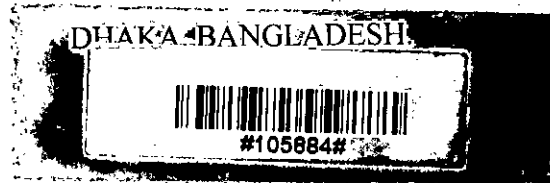
THE DEGREE

OF

MASTER OF SCIENCE IN ENGINEERING (ELECTRICAL AND ELECTRONIC)



DEPARTMENT OF ELECTRICAL AND ELECTRONIC ENGINEERING  
BANGLADESH UNIVERSITY OF ENGINEERING AND TECHNOLOGY (BUET),




JULY, 2008

## CERTIFICATE



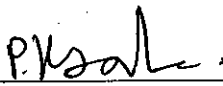
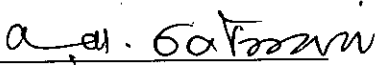
This is to certify that this work has been done by me and has not been submitted elsewhere for the award of any degree or diploma.

Signature of the candidate

  
\_\_\_\_\_ 20.07.08  
(Bindubritta Acharjee)

The thesis titled, "Analysis of a Wire Antenna by Solving Pocklington's Integral Equation Using Wavelets," submitted by Bindubritta Acharjee of M. Sc. Engineering (EEE) Roll No. 040506208F of the session April 2005, has been accepted as satisfactory for partial fulfillment of the requirements for the degree of M. Sc. Engineering (Electrical and Electronic) on July 27, 2008.

### BOARD OF EXAMINERS

1.   
**Dr. Md. Abdul Matin** 27.7.08  
 Professor  
 Department of Electrical and Electronic Engineering,  
 Bangladesh University of Engineering and Technology  
 (BUET), Dhaka-1000.  
 Chairman  
 (Supervisor)
2.   
**Dr. Aminul Hoque** 27/7/08  
 Professor and Head  
 Department of Electrical and Electronic Engineering,  
 Bangladesh University of Engineering and Technology  
 (BUET), Dhaka-1000.  
 Member  
 (Ex-Officio)
3.   
**Dr. Pran Kanai Saha** 27.7.08  
 Professor  
 Department of Electrical and Electronic Engineering,  
 Bangladesh University of Engineering and Technology  
 (BUET), Dhaka-1000.  
 Member
4.   
**Dr. Abdul Matin Patwari** 27/7/08  
 Vice-chancellor,  
 University of Asia Pacific (UAP),  
 House No. 49/C, Road No. 4A,  
 Dhanmondi R/A, Dhanmondi, Dhaka-1209.  
 Member  
 (External)

### ACKNOWLEDGEMENT

It is a matter of a great pleasure to acknowledge author's deep indebtedness to his supervisor Dr. Md. Abdul Matin, Professor, Department of Electrical and Electronic Engineering, Bangladesh University of Engineering and Technology (BUET), Dhaka for all of his advice, constant support and motivation throughout the completion of this research work.

The author would also acknowledge sincere thanks to other members of the board, Dr. Aminul Haque, Professor and Head, Department of Electrical and Electronic Engineering, BUET, Dhaka; Dr. Pran Kanai Saha, Professor, Department of Electrical and Electronic Engineering, BUET, Dhaka and Dr. Abdul Matin Patwari, Honorable Vice-chancellor, University of Asia Pacific (UAP), Dhaka; for their valuable suggestions and encouragement.

Finally, the author would like to thank all who were involved directly or indirectly in successful completion of this work.

### ABSTRACT

Solving Pocklington's integral equation for the thin and straight wire antennas by moment method, the current distributions of a half-wave and a full-wave dipole have been deduced using semi-orthogonal wavelet bases that are constructed from the second-order cardinal B-spline. The results agree well with those obtained by King's Three-term Approximation and with the measured values of Mack. The current distributions have been calculated in different scale and with respect to the computing time, the most efficient scale for analysis has been determined. The method is then extended for antenna array analysis. Current distributions on each antenna of a three-element Yagi-Uda array have been derived and compared with those based on King's Three-term Approximation. With the corresponding current distribution, the input impedance and radiation pattern of thin and straight wire antennas and the properties of a three-element Yagi-Uda array have been calculated, compared with theoretical results and found physically significant.

**TABLE OF CONTENTS**

<b>CHAPTER – 1</b>	<b>INTRODUCTION AND BACKGROUND .....</b>	<b>1</b>
1.1	Antenna .....	2
1.2	Why Antennas Radiate .....	2
1.3	Background .....	4
1.4	Objectives of the Thesis .....	4
1.5	Thesis Layout .....	5
<b>CHAPTER – 2</b>	<b>CURRENT DISTRIBUTION ALONG A WIRE ANTENNA .....</b>	<b>6</b>
2.1	Outline of the Method of Analysis .....	7
2.2	Current Distribution of a Transmitting Half-wave Dipole Antenna .....	9
2.3	Current Distribution of a Receiving Half-wave Dipole Antenna .....	16
2.4	Comparison with Mack's and King's Values for Half-wave Dipole .....	19
2.5	Current Distribution of a Full-wave Transmitting Dipole .....	20
2.6	Comparison with Mack's and King's Values for Full-wave Dipole .....	24
2.7	Discussion .....	25
<b>CHAPTER – 3</b>	<b>CURRENT DISTRIBUTION OF A WIRE IN A YAGI-UDA ARRAY</b>	<b>26</b>
3.1	General Formulation .....	27
3.2	Current Distribution of a Three-element Yagi-Uda Array .....	28
3.3	Comparison with King's Three-term Approximation .....	32
3.4	Discussion .....	34
<b>CHAPTER – 4</b>	<b>INPUT IMPEDANCE OF THE WIRE ANTENNA .....</b>	<b>35</b>
4.1	General Formulation .....	36
4.2	Impedance of the Linear Wire Antenna and Array .....	36
4.3	Discussion .....	36
<b>CHAPTER – 5</b>	<b>FAR-FIELD RADIATION PATTERN OF THE WIRE ANTENNA ...</b>	<b>37</b>
5.1	General Formulation .....	38
5.2	Far-field Radiation Pattern for the Linear Wire Antenna .....	38
5.3	Far-field Radiation Pattern for the Antenna Array .....	40
5.4	Discussion .....	43
<b>CHAPTER – 6</b>	<b>GENERAL DISCUSSION .....</b>	<b>44</b>
6.1	General Discussion .....	45
6.2	Further Scope of Work .....	45
<b>APPENDICES</b>		
APPENDIX – A	Physical Constants, Relative Error .....	46
APPENDIX – B	Computer Programs .....	47
APPENDIX – C	Wavelets .....	64
APPENDIX – D	Moment Method .....	67
APPENDIX – E	Gauss Quadrature .....	68
APPENDIX – F	LU Factorization .....	69
<b>REFERENCES .....</b>		<b>70</b>

## TABLE OF FIGURES

Fig. 2.1	Thin-wire model of cylindrical antenna .....	7
Fig. 2.2	Scale functions of the wavelets at scale = 2 .....	10
Fig. 2.3	Wavelet functions of the wavelets at scale = 2 .....	11
Fig. 2.4	Current distributions along the half-wave transmitting dipole at different scales .....	12
Fig. 2.5	Current distribution along the half-wave dipole at scale = 2 .....	13
Fig. 2.6	Current distribution along the half-wave dipole at scale = 3 .....	13
Fig. 2.7	Current distribution along the half-wave dipole at scale = 4 .....	14
Fig. 2.8	Current distribution along the half-wave dipole at scale = 5 .....	14
Fig. 2.9	CPU time for complete analysis of half-wave dipole at different scales .....	15
Fig. 2.10	Current distributions along the half-wave receiving dipole at scale = 2 & 3 .....	16
Fig. 2.11	Current distributions for half-wave receiving dipole at scale = 3 & 4 by Nevels .....	17
Fig. 2.12	Comparison of transmitting (Tx) & receiving (Rx) half-wave dipole current .....	18
Fig. 2.13	Comparison of current distributions for the half-wave dipole at scale = 3 .....	19
Fig. 2.14	Current distributions along the full-wave transmitting dipole at different scales .....	20
Fig. 2.15	Current distribution along the full-wave dipole at scale = 2 .....	21
Fig. 2.16	Current distribution along the full-wave dipole at scale = 3 .....	21
Fig. 2.17	Current distribution along the full-wave dipole at scale = 4 .....	22
Fig. 2.18	CPU time for complete analysis of full-wave dipole at different scales .....	23
Fig. 2.19	Comparison of current distributions for a full-wave dipole at scale = 4 .....	24
Fig. 3.1	Three-element Yagi-Uda array .....	27
Fig. 3.2	Current distribution along the active dipole at scale = 3 .....	29
Fig. 3.3	Current distribution along the reflector at scale = 3 .....	30
Fig. 3.4	Current distribution along the director at scale = 3 .....	31
Fig. 3.5	Comparison of current distributions for the active dipole at scale = 3 .....	32
Fig. 3.6	Comparison of current distributions for the reflector at scale = 3 .....	33
Fig. 3.7	Comparison of current distributions for the director at scale = 3 .....	34
Fig. 5.1	Azimuthal pattern of the half-wave dipole in absolute units .....	39
Fig. 5.2	Azimuthal pattern of the full-wave dipole in absolute units .....	40
Fig. 5.3	E-plane pattern of the Yagi-Uda array in absolute units .....	41
Fig. 5.4	Magnified rear view of the E-plane pattern of the Yagi-Uda array .....	41
Fig. 5.5	H-plane pattern of the Yagi-Uda array in absolute units .....	42
Fig. 5.6	Magnified rear view of the H-plane pattern of the Yagi-Uda array .....	42
Fig. 5.7	Comparison for azimuthal pattern of the half-wave, full-wave and Yagi-Uda array ...	43



## CHAPTER – 1

### INTRODUCTION AND BACKGROUND



## 1.1 Antenna

An antenna is a transducer that converts electromagnetic radiations into electrical currents or vice-versa, depending on whether it is being used for receiving or for transmitting electromagnetic wave. Antenna is a basic component of any electronic system which depends on free space as the propagation medium. The official IEEE definition of an antenna as given by Stutzman and Thiele [1] follows the concept: "The part of a transmitting or receiving system that is designed to radiate or receive electromagnetic waves."

## 1.2 Why Antennas Radiate

Any charged particle produces an electric field  $\vec{E}$  that is infinite in extent and depending on the nature of its charge the field can be pointed inward or outward. The only magnetic field associated with the stationary charged particle is its spin magnetic dipole moment which can be ignored in this case. Therefore, the  $\vec{E}$  field remains same over time and stores the particle's electromagnetic energy when no other charged particles are present. When another charge is present, the field impacts a force on each other and energy is transferred. As per Coulomb's Law [1780], at a distance  $r$  the electric field  $\vec{E}$  for a charged particle with charge  $q$  can be found as –

$$\vec{E} = \vec{E}_{static} = \hat{r} \frac{1}{4\pi\epsilon_0} \frac{q}{r^2} \quad (1.2.1)$$

where,  $\epsilon_0$  is the permittivity of the space.

But, when the particle moves with a velocity  $\vec{v}$ , its field becomes dynamic. The dynamic  $\vec{E}$  field seen to a stationary observer can be determined by Lorentz transformation [1905] as –

$$\vec{E} = \vec{E}_{dynamic} = \hat{r} \frac{1}{4\pi\epsilon_0} \frac{q}{r^2} \frac{1-(v^2/c^2)}{[1-(v^2/c^2)\sin^2\theta]^{3/2}} \quad (1.2.2)$$

where,  $\theta$  is the angle between the  $\vec{E}$  field and the particles direction of travel, and  $c$  is the speed of light.

The dynamic  $\vec{E}$  field raises a  $\vec{B}$  field with magnitude–

$$|\vec{B}| = \frac{1}{c^2} |\vec{v} \times \vec{E}| = \frac{1}{4\pi\epsilon_0} \frac{q}{r^2} \frac{1-(v^2/c^2)}{[1-(v^2/c^2)\sin^2\theta]^{3/2}} \frac{v \sin\theta}{c^2} \quad (1.2.3)$$

Hence, in free space for a moving charged particle with a constant velocity and no external influences, a stationary observer will observe a constant-magnitude electric and

magnetic fields are present simultaneously where the  $\vec{B}$  vector is perpendicular to both the  $\vec{E}$  vector and also to the velocity vector  $\vec{v}$ .

When a constant voltage source is connected across the length of a wire, the voltage causes a proportional current, governed by Ohm's law [1827] ( $I = V/R$ ). The total number of electrons is equal to the total number of protons in the wire. But as protons are fixed in the lattice of the wire, the constant current traveling in that wire consists of migrating electrons only. Although the path of each individual electron is random and complex, the average movement of the electrons, can be considered as a group, causes a constant drift of charge. Therefore, at macroscopic level the current can be considered as a fictitious charge that traveling at a constant velocity. Experiments have confirmed that, constant current flow in a wire produces only an observable magnetic field  $\vec{B}$ , but no electric field  $\vec{E}$  at all. This because the protons produce a static radial  $\vec{E}$  field which is uniform along the wire and produce no  $\vec{B}$  field as there is no relative motion with respect to the observer. On the other hand, the migrating electrons produce both  $\vec{E}$  and  $\vec{B}$  field. The electrostatic  $\vec{E}$  field from all the protons and electrons cancel each other and just left the  $\vec{B}$  field.

Field lines of particles moving at constant velocities do not bend. But, when a charge particle accelerates, the lines of the electric field start to bend and the bent field lines of the charge correspond to radiating energy. Einstein's theory of relativity [1905] helps to explain the phenomenon. If a charge particle is suddenly created, its field would not instantly appear everywhere. The field would first appear immediately around the particle and then extend outward at the speed of light. As a particle moves, the surrounding field continually updates to its new position, but this information can propagate only at the speed of light. Points in the space surrounding the particle actually experience the field corresponding to where the particle used to be. This delay is known as time retardation. Even a charge moving at constant velocity should cause the field lines to bend due to the time retardation. The electromagnetic field gets around the delay by predicting where the particle will be based on its past velocity. So, if there is no change in velocity, the lines of the electric field become curl-free.

The curly field lines of a charge correspond to radiated energy. This phenomenon can be analyzed from the kinetic-energy perspective. To accelerate a particle, force is needed and the force transfers energy to the particle increasing its kinetic energy. Similarly, to accelerate a charged particle, required force accelerate its field and this energy propagates outwards as a wave.

When, electrons in an antenna accelerate because of the application of some time-varying electromotive force or voltage to the antenna; each electronic charge  $q$  in the antenna experiences a force,  $\vec{F} = q \vec{E}$  and therefore accelerates according to  $\vec{F} = m \vec{a}$ , where  $m$  is the mass of the electron and  $\vec{a}$  is the acceleration. Thus we have an alternating current in the antenna which raises an alternating  $\vec{B}$  field. The alternating  $\vec{B}$  field induces an alternating  $\vec{E}$  field to counteract the change in field producing it; which is known as

Lenz's effect [1834]. When the current in the wire alternates rapidly enough; the alternating  $\vec{B}$  field propagates away at speed  $c$  before the Lenz effect can cancel it. Thus both  $\vec{E}$  field and  $\vec{B}$  field are radiated from the antenna. The radiated  $\vec{B}$  field is perpendicular to the antenna while the  $\vec{E}$  field is parallel to it.

### 1.3 Background

Analysis of electromagnetic radiation, scattering from material bodies and wave propagation in a dispersive medium were formulated by James Clerk Maxwell [2] in 1864, which provide the foundation of classical electromagnetism. In 1887 Hertz [3] experimentally verified the wave phenomena consequent to Maxwell's equations. In 1897 Pocklington [4] extended the insights of Lorentz [5] and Hertz [3] by deducing an integral equation for the current along a cylindrical conductor. The equation is well known as Pocklington's integral equation and it forms the basis of linear wire antenna analysis. But due to the highly singular kernel, no attempt was made till 1937 for analytical solution of the equation to determine the actual current distribution. Instead, a convenient sinusoidal distribution was assumed for the half-wave dipole by Carter [6] in 1932 and for an antenna with arbitrary length by Brown [7] in 1937. However, leading to infinite impedance for an one-wavelength antenna, approximate solutions of the integral equation have been resolved by L. V. King [8] in 1937, by Hallén [9] in 1938, by King [10] in 1965 and continuing to the present. Among the various analytical methods some permit successive improvement; e.g. iteration method applied by King and Middleton [11], Fourier series expansion of the current distribution by Duncan and Hinchey [12], moment method for electrically short antenna by Harrington [13], generalized ray method for high-frequency analysis by Burkholder [14] and so on. In the moment method using conventional bases the resultant impedance matrix becomes dense. Hence the inversion and final solution of the system is very time consuming. To overcome the huge memory requirement and computation time, wavelet bases was first proposed by Beylkin, Coifman and Rokhlin [15]. However, using orthogonal wavelet bases the matrix is dense yet. Thus Chui and Quak [16] used wavelets on a bounded interval; Nevels, Goswami and Tehrani [17] used semi-orthogonal spline wavelets; Tretiakov and Pan [18] used discrete wavelet packet to solve Pocklington's equation by moment method. However, in moment method, the number of unknowns for the sub-domain bases is less than the wavelet bases. Appropriate scaling of the basis function might improve the scenario. But how to choose such a scaled wavelet basis for a general geometry is still an open question.

### 1.4 Objectives of the Thesis

The objectives of the thesis are – to calculate the current distributions along the length of a center-fed transmitting half-wave, full-wave and a receiving half-wave thin wire dipole antennas; and along the length of each antenna of a three-element (reflector, active dipole and director) Yagi-Uda array by solving Pocklington's integral equation using semi-orthogonal B-spline wavelets in the moment method. To calculate the current function at

different scales and to choose the appropriate scale with respect to the computing time. To compare the results with experimental values obtained by Mack [19] and with King's Three-term theory. To calculate the antenna input impedance and far-field radiation pattern of each antenna.

## 1.5 Thesis Layout

The thesis covers the calculation of the antenna current distribution and determination of some antenna properties using the calculated current distribution. In chapter – 2, current distribution of a half-wave linear dipole (both transmitting and receiving) antenna and a transmitting full-wave dipole antenna have been calculated at different scales. Appropriate scale for analysis has been chosen and the current distributions at that scale have been compared with King's Three-term theory and Mack's experimental values. In chapter – 3, current distribution along the length of each antenna of a three-element Yagi-Uda array have been calculated at different scale. Results of appropriate scale have been compared with King's Three-term theoretical values. In chapter – 4, input impedance of each antenna have been determined and also compared with experimental and theoretical values. In chapter – 5, radiation pattern of each antenna have been determined and compared with each other. Finally a general discussion has been presented in chapter – 6.

## **CHAPTER – 2**

### **CURRENT DISTRIBUTION ALONG A WIRE ANTENNA**

## 2.1 Outline of the Method of Analysis

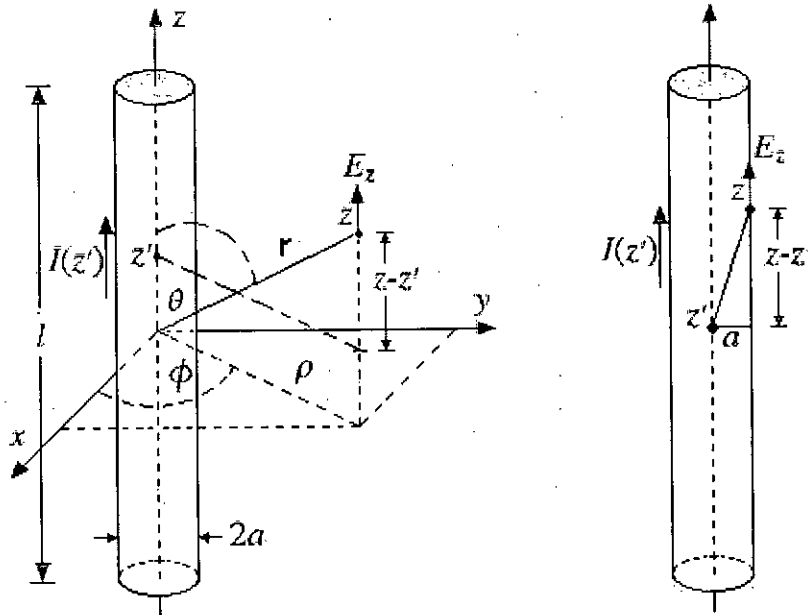


Fig. 2.1 Thin-wire model of cylindrical antenna

For a  $z$ -directed thin cylindrical wire antenna, as shown in Fig. 2.1 of length  $l$  and radius  $a$ , with a current distribution  $I(z')$  along its length; the Pocklington's integral equation is written as –

$$\frac{j\eta\lambda}{8\pi^2} \int_{-l/2}^{l/2} I_z(z') \left( \frac{\partial^2}{\partial z^2} + k^2 \right) \frac{e^{-jk\sqrt{(z-z')^2 + a^2}}}{\sqrt{(z-z')^2 + a^2}} dz' = E_z^{in}(z) \quad (2.1.1)$$

where,  $\eta = \sqrt{(\mu_0/\epsilon_0)}$ ,  $k = 2\pi/\lambda$ .  $\mu_0$  is the permeability,  $\epsilon_0$  is the permittivity of space and  $\lambda$  is the wavelength.  $E^{in}(z)$  is the incident field, which induces the current in the antenna. For a transmitting antenna,  $E^{in}(z) = V_0/\Delta z$ , where  $V_0$  is the applied voltage within a short gap  $\Delta z$  of antenna length and for a receiving antenna with a uniform plane wave  $E_0$  incident at a polar angle  $\theta$ ,  $E^{in}(z) = E_0 \sin\theta e^{jkz \cos\theta}$ ; where the propagation vector  $\vec{k}$  is coplanar with the antenna axis. The magnetic vector potential of the antenna will be  $z$ -directed as –

$$\vec{A}(\vec{r}) = \hat{z} \frac{\mu}{4\pi} \int_{-l/2}^{l/2} I_z(z') \frac{e^{-jk\sqrt{(z-z')^2 + a^2}}}{\sqrt{(z-z')^2 + a^2}} dz' \quad (2.1.2)$$

Now, to expand the unknown current function  $I_z(z')$ , semi-orthogonal wavelet bases constructed from the second-order cardinal B-spline, can be used.

The scaling functions, which are implemented only at the lowest scale (scale = 2), contain all frequency information about the current below the scale, are given by –

$$\phi_{2,q} = \begin{cases} z_2 - q; & z_2 \in [q, q+1] \\ 2 - (z_2 - q); & z_2 \in [q+1, q+2] \end{cases} \quad (2.1.3)$$

where,  $q = 0, 1$  and  $2$ .

And the wavelets are given by –

$$\psi_{p,q} = \frac{1}{6} \begin{cases} z_p - q; & z_p \in [q, q+0.5] \\ 4 - 7(z_p - q); & z_p \in [q+0.5, q+1] \\ -19 + 16(z_p - q); & z_p \in [q+1, q+1.5] \\ 29 - 16(z_p - q); & z_p \in [q+1.5, q+2] \\ -17 + 7(z_p - q); & z_p \in [q+2, q+2.5] \\ 3 - (z_p - q); & z_p \in [q+2.5, q+3] \end{cases} \quad (2.1.4)$$

where,  $p$  is the respective scale ( $\geq 2$ ) and  $q = 0, \dots, 2^p - 3$ .

The actual coordinate position  $z'$  is related to  $z_p$  according to –

$$z_p = 2^p \left[ \frac{z' + l/2}{l} \right] \quad (2.1.5)$$

Hence, the current function can be expressed as –

$$I_z(z') = \sum_{q=0}^2 c_{2,q} \phi_{2,q}(z') + \sum_{p=2}^{p_n} \sum_{q=0}^{2^p-3} d_{p,q} \psi_{p,q}(z') \quad (2.1.6)$$

Substituting the current expression in Pocklington's integral equation (2.1.1) we obtain –

$$\sum_{q=0}^2 c_{2,q} \int_{-l/2}^{l/2} Z(z, z') \phi_{2,q}(z') dz' + \sum_{p=2}^{p_n} \sum_{q=0}^{2^p-3} d_{p,q} \int_{-l/2}^{l/2} Z(z, z') \psi_{p,q}(z') dz' = E_z^m(z) \quad (2.1.7)$$

where,

$$\begin{aligned} Z(z, z') &= \frac{j\eta\lambda}{8\pi^2} \left( \frac{\partial^2}{\partial z^2} + k^2 \right) \frac{e^{-jk\sqrt{(z-z')^2 + a^2}}}{\sqrt{(z-z')^2 + a^2}} \\ &= -\frac{3j\eta\lambda a^2}{8\pi^2} \left[ \frac{e^{-jk\sqrt{(z-z')^2 + a^2}}}{\left( \sqrt{(z-z')^2 + a^2} \right)^5} \right] + \frac{3\eta\lambda k a^2}{8\pi^2} \left[ \frac{e^{-jk\sqrt{(z-z')^2 + a^2}}}{\left( \sqrt{(z-z')^2 + a^2} \right)^4} \right] \\ &\quad + \frac{j\eta\lambda (2 + k^2 a^2)}{8\pi^2} \left[ \frac{e^{-jk\sqrt{(z-z')^2 + a^2}}}{\left( \sqrt{(z-z')^2 + a^2} \right)^3} \right] - \frac{\eta\lambda k}{4\pi^2} \left[ \frac{e^{-jk\sqrt{(z-z')^2 + a^2}}}{\left( \sqrt{(z-z')^2 + a^2} \right)^2} \right] \end{aligned} \quad (2.1.8)$$

Applying Galerkin's technique in (2.1.7) we have –

$$\begin{aligned} & \sum_{q=0}^2 c_{2,q} \int_{-l/2}^{l/2} \int_{-l/2}^{l/2} Z(z, z') \phi_{2,q}(z') \phi_{2,m}(z) dz' dz \\ & + \sum_{p=2}^{p_u} \sum_{q=0}^{2^p-3} d_{p,q} \int_{-l/2}^{l/2} \int_{-l/2}^{l/2} Z(z, z') \psi_{p,q}(z') \phi_{2,m}(z) dz' dz = \int_{-l/2}^{l/2} E_z^{in}(z) \phi_{2,m}(z) dz \end{aligned} \quad (2.1.9)$$

where,  $m \in (0, 2^{iu} - 3)$ .

$$\begin{aligned} & \sum_{q=0}^2 c_{2,q} \int_{-l/2}^{l/2} \int_{-l/2}^{l/2} Z(z, z') \phi_{2,q}(z') \psi_{i,m}(z) dz' dz \\ & + \sum_{p=2}^{p_u} \sum_{q=0}^{2^p-3} d_{p,q} \int_{-l/2}^{l/2} \int_{-l/2}^{l/2} Z(z, z') \psi_{p,q}(z') \psi_{i,m}(z) dz' dz = \int_{-l/2}^{l/2} E_z^{in}(z) \psi_{i,m}(z) dz \end{aligned} \quad (2.1.10)$$

where,  $i \in (2, i_u)$ ,  $m \in (0, 2^{iu} - 3)$ ; and

These equations can be written in a compact matrix form as –

$$\begin{pmatrix} Zg_{0,0} & Zg_{0,1} & \dots & Zg_{0,n} & \dots & Zg_{0,2^{p_u}+1} \\ Zg_{1,0} & Zg_{1,1} & \dots & Zg_{1,n} & \dots & Zg_{1,2^{p_u}+1} \\ \dots & \dots & \dots & \dots & \dots & \dots \\ Zg_{n,0} & Zg_{n,1} & \dots & Zg_{n,n} & \dots & Zg_{n,2^{p_u}+1} \\ \dots & \dots & \dots & \dots & \dots & \dots \\ Zg_{2^{p_u}+1,0} & Zg_{2^{p_u}+1,1} & \dots & Zg_{2^{p_u}+1,n} & \dots & Zg_{2^{p_u}+1,2^{p_u}+1} \end{pmatrix} \cdot \begin{pmatrix} c_{2,0} \\ c_{2,1} \\ \dots \\ d_{p,q} \\ \dots \\ d_{p_u,2^{p_u}+1} \end{pmatrix} = \begin{pmatrix} Eg_0 \\ Eg_1 \\ \dots \\ Eg_n \\ \dots \\ Eg_{2^{p_u}+1} \end{pmatrix} \quad (2.1.11)$$

Solving the matrix the unknown current coefficients can be calculated to deduce the current distribution  $I_z(z')$ .

## 2.2 Current Distribution of a Transmitting Half-wave Dipole Antenna

Let us consider, a z-directed cylindrical half wave dipole antenna driven by a voltage source and operating at 300 MHz in free space. Therefore –

The permeability,  $\mu_0 = 4\pi \times 10^{-7}$  H/m

The permittivity,  $\epsilon_0 = 8.854 \times 10^{-2}$  F/m

The characteristics wave impedance,  $\eta = 376.73$ .

The wave number,  $k = 6.283$ ; i.e.  $k_0 h = \pi/2$ , where,  $h$  = half-length of antenna

The antenna radius,  $a = 7.022 \times 10^{-3} \lambda = \Delta z$

The input voltage level,  $V_0 = 1$  Volt.



Now, considering the second-order B-spline, from equation (2.1.3) the scaling functions at lowest scale ( $s_0 = 2$ ) become –

$$\begin{aligned}\phi_{2,0}(z') &= 8z' + 2 && ; -0.25 \leq z' \leq -0.125 \\ &= -8z' && ; -0.125 \leq z' \leq 0 \\ &= 0 && ; \textit{elsewhere}\end{aligned}\tag{2.2.1}$$

$$\begin{aligned}\phi_{2,1}(z') &= 8z' + 1 && ; -0.125 \leq z' \leq 0 \\ &= 1 - 8z' && ; 0 \leq z' \leq 0.125 \\ &= 0 && ; \textit{elsewhere}\end{aligned}\tag{2.2.2}$$

$$\begin{aligned}\phi_{2,2}(z') &= 8z' && ; 0 \leq z' \leq 0.125 \\ &= 2 - 8z' && ; 0.125 \leq z' \leq 0.25 \\ &= 0 && ; \textit{elsewhere}\end{aligned}\tag{2.2.3}$$

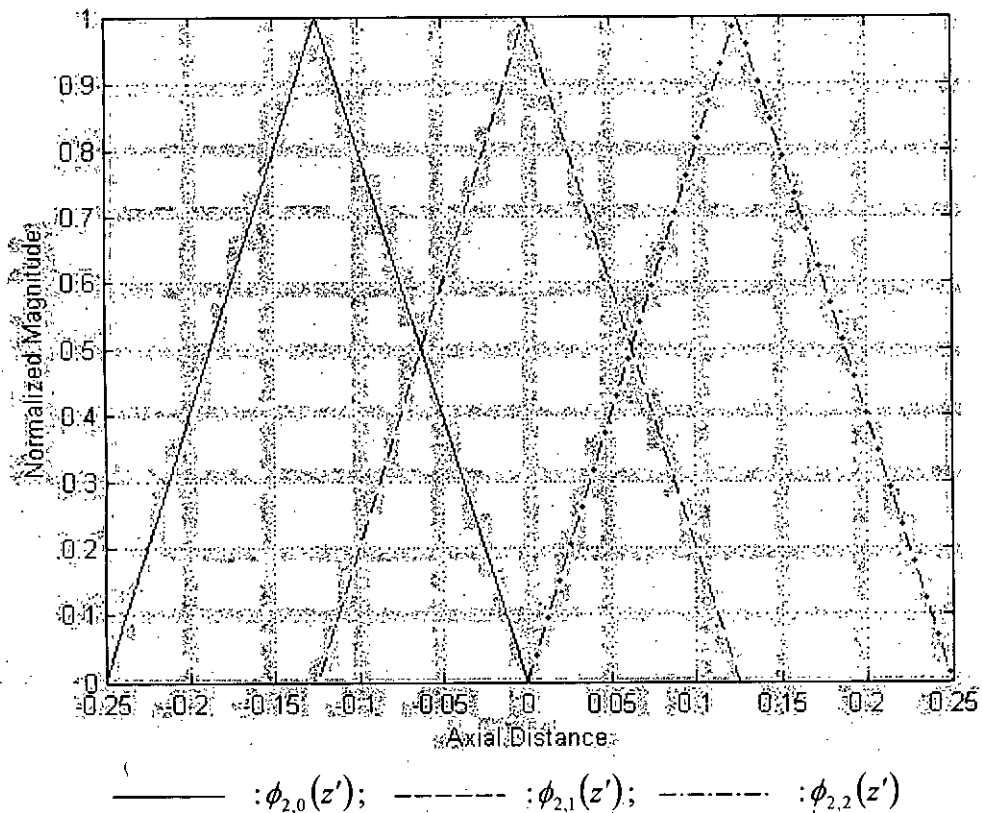


Fig. 2.2 Scale functions of the wavelets at scale = 2

And from equation (2.1.4) at lowest scale ( $s_0 = 2$ ) the wavelet functions become –

$$\begin{aligned}
 \psi_{2,0}(z') &= 1.33z' + 0.33 && ; -0.25 \leq z' \leq -0.1875 \\
 &= -9.33z' - 1.67 && ; -0.1875 \leq z' \leq -0.125 \\
 &= 21.33z' + 2.17 && ; -0.125 \leq z' \leq -0.0625 \\
 &= -21.33z' - 0.5 && ; -0.0625 \leq z' \leq 0 \\
 &= 9.33z' - 0.5 && ; 0 \leq z' \leq 0.0625 \\
 &= -1.33z' + 0.17 && ; 0.0625 \leq z' \leq 0.125 \\
 &= 0 && ; \textit{elsewhere}
 \end{aligned}
 \tag{2.2.4}$$

$$\begin{aligned}
 \psi_{2,1}(z') &= 1.33z' + 0.17 && ; -0.125 \leq z' \leq -0.0625 \\
 &= -9.33z' - 0.5 && ; -0.0625 \leq z' \leq 0 \\
 &= 21.33z' - 0.5 && ; 0 \leq z' \leq 0.0625 \\
 &= -21.33z' + 2.17 && ; 0.0625 \leq z' \leq 0.125 \\
 &= 9.33z' - 1.67 && ; 0.125 \leq z' \leq 0.1875 \\
 &= -1.33z' + 0.33 && ; 0.1875 \leq z' \leq 0.25 \\
 &= 0 && ; \textit{elsewhere}
 \end{aligned}
 \tag{2.2.5}$$

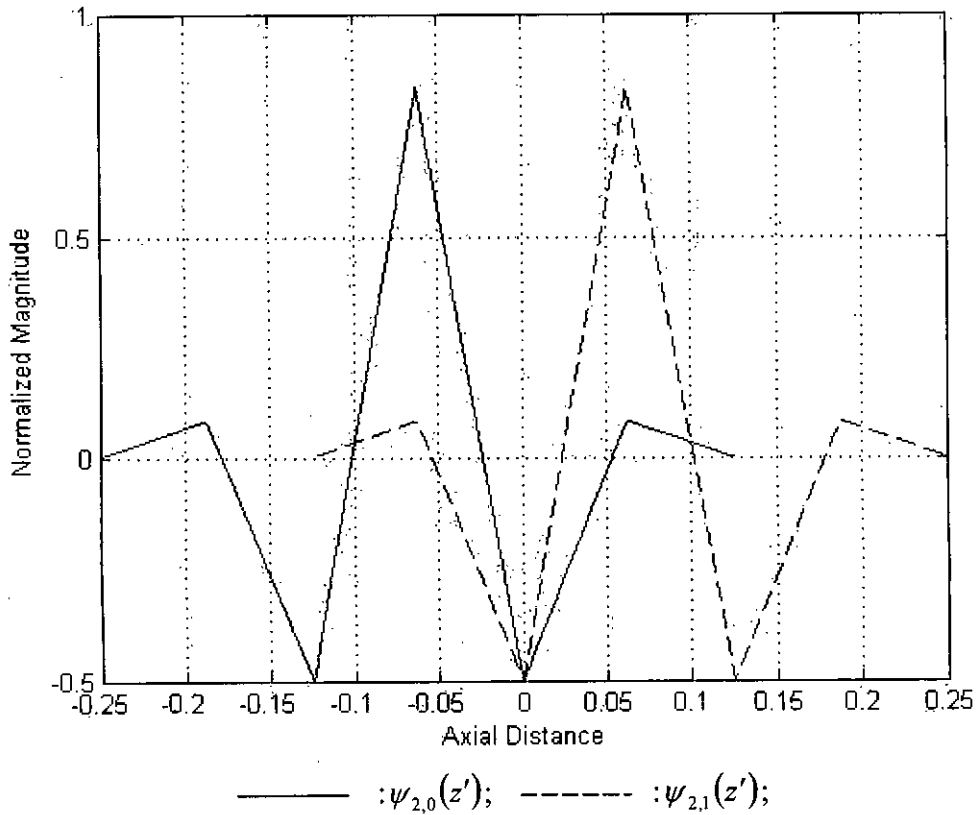


Fig. 2.3 Wavelet functions of the wavelets at scale = 2

Hence, as per equation (2.1.6), the current function is –

$$I_z(z') = c_{2,0} \phi_{2,0}(z') + c_{2,1} \phi_{2,1}(z') + c_{2,2} \phi_{2,2}(z') + d_{2,0} \psi_{2,0}(z') + d_{2,1} \psi_{2,1}(z') \quad (2.2.6)$$

and the integral equation (2.1.7) becomes –

$$\begin{aligned} c_{2,0} \int_{-1/2}^{1/2} Z(z, z') \phi_{2,0}(z') dz' + c_{2,1} \int_{-1/2}^{1/2} Z(z, z') \phi_{2,1}(z') dz' + c_{2,2} \int_{-1/2}^{1/2} Z(z, z') \phi_{2,2}(z') dz' \\ + d_{2,0} \int_{-1/2}^{1/2} Z(z, z') \psi_{2,0}(z') dz' + d_{2,1} \int_{-1/2}^{1/2} Z(z, z') \psi_{2,1}(z') dz' = E_z^{in}(z) \end{aligned} \quad (2.2.7)$$

Now, applying Galerkin's technique in this equation and solving the value of the integrated matrix elements, the matrix has been constructed. Solving the matrix equation the current distributions at different scales have been calculated.

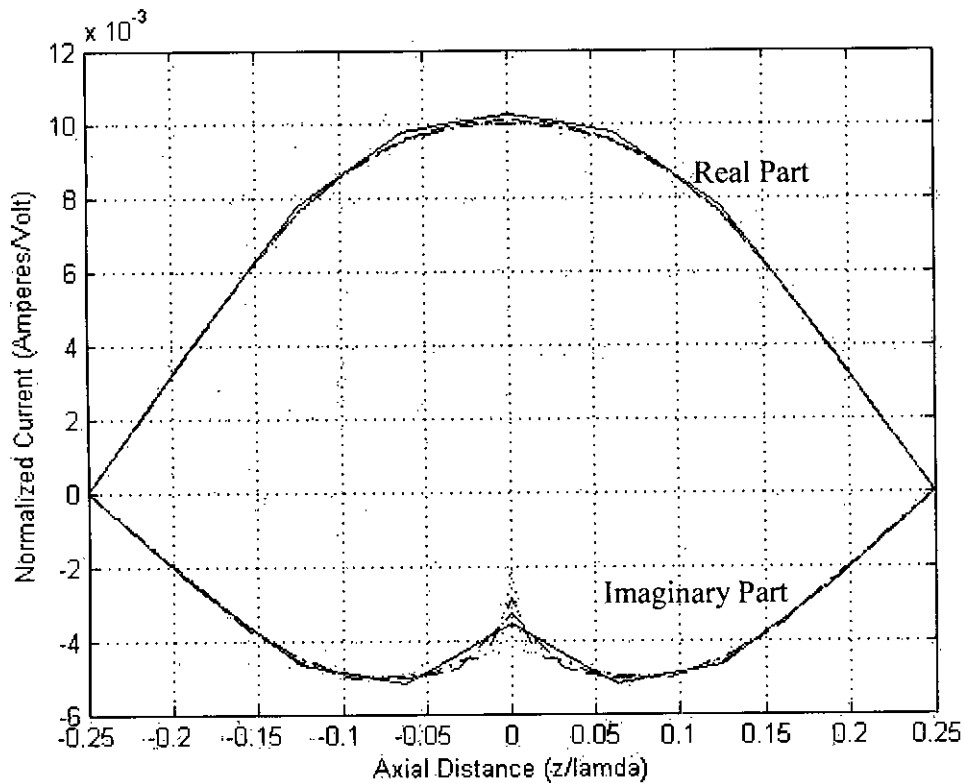


Fig. 2.4 Current distributions along the half-wave transmitting dipole at different scales

Current distributions along the half-wave transmitting dipole at different scales are shown in figure 2.4. But, the results are so close that the variation with respect to different scale can not be distinguished. So in next pages, results at each scale have been provided for better understanding.

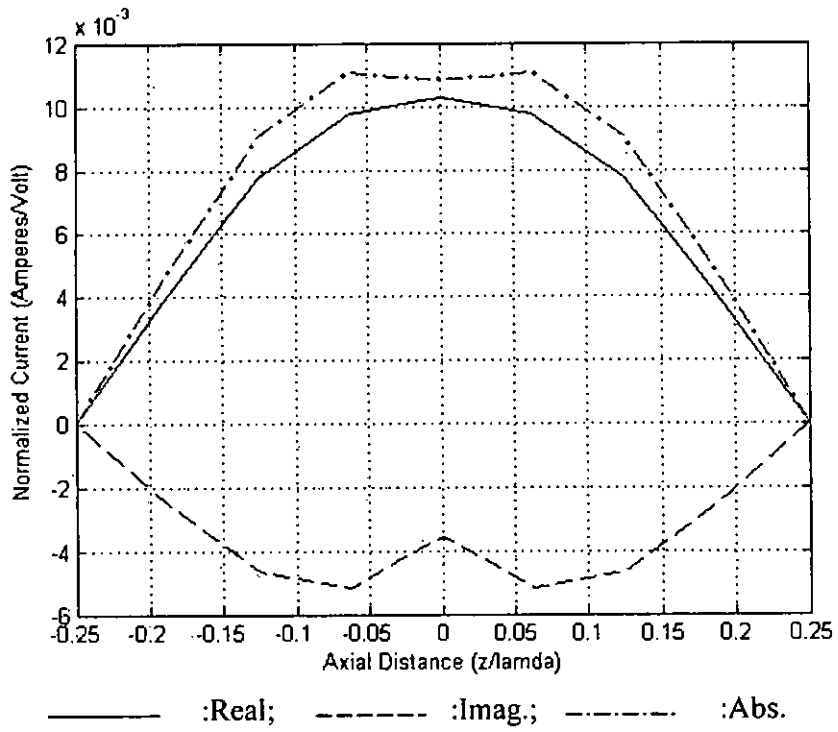


Fig. 2.5 Current distribution along the half-wave dipole at scale = 2

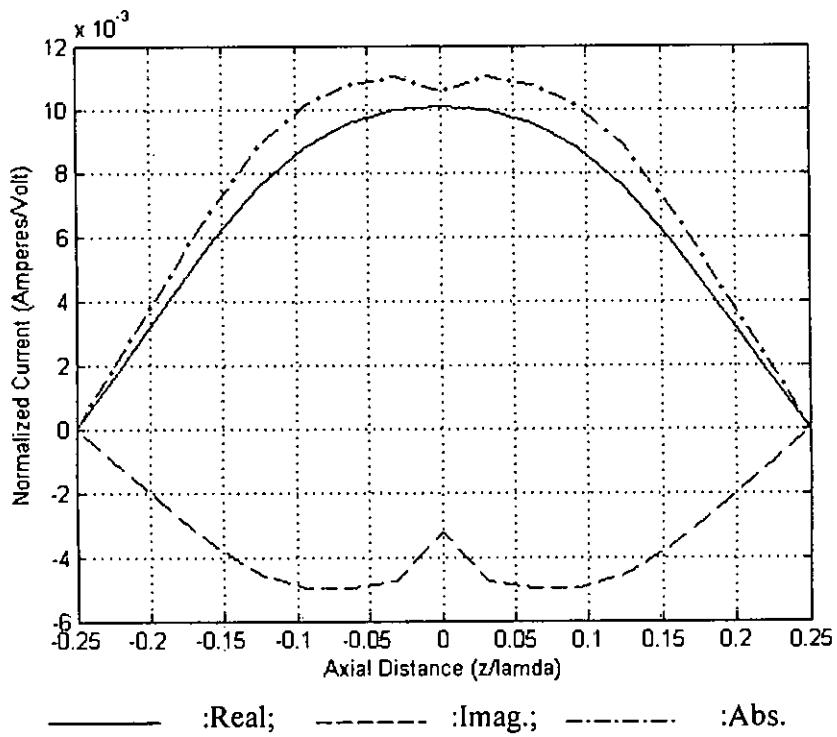


Fig. 2.6 Current distribution along the half-wave dipole at scale = 3

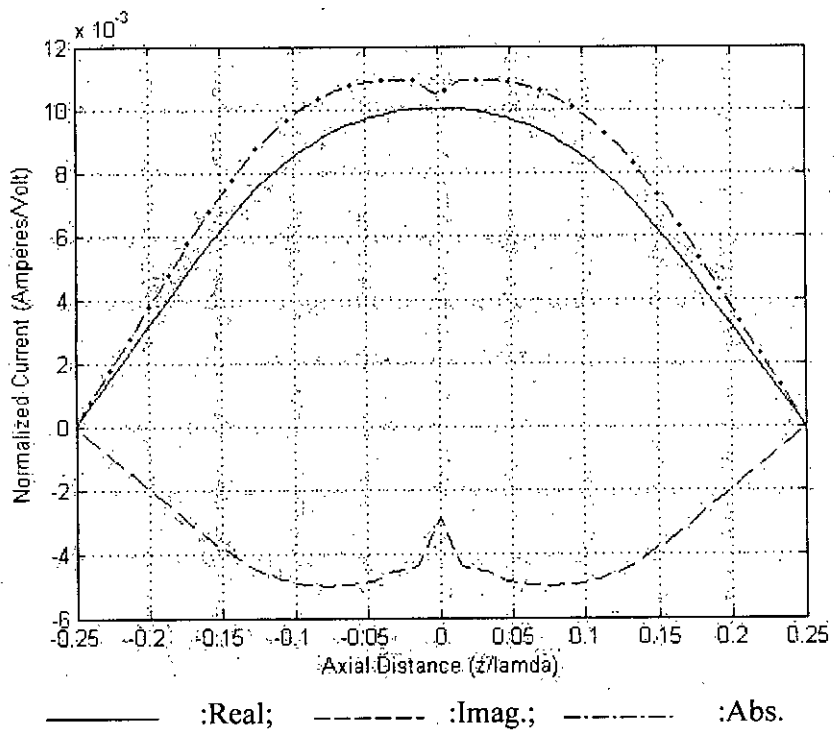


Fig. 2.7 Current distribution along the half-wave dipole at scale = 4

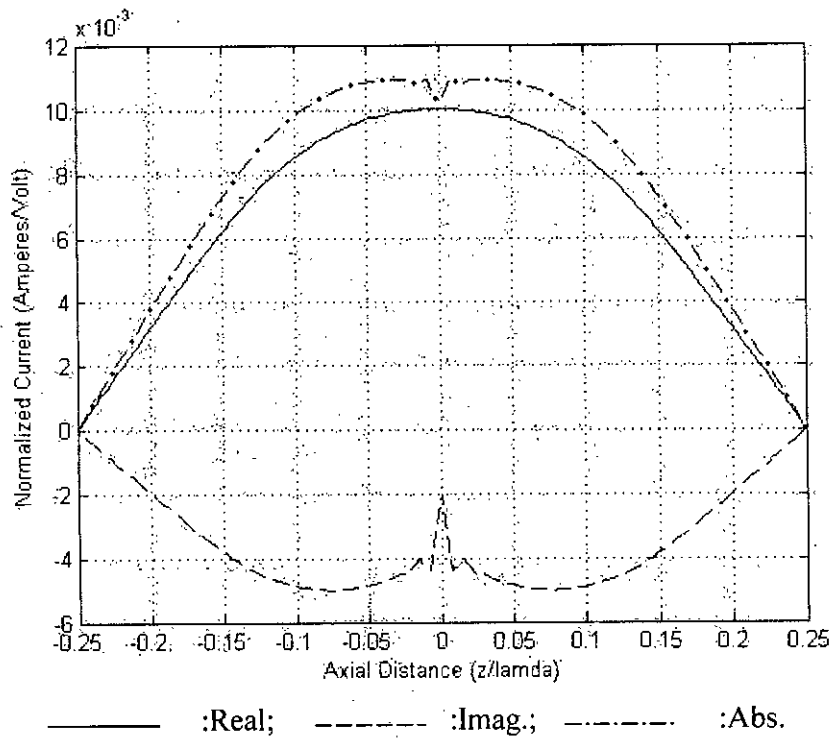


Fig. 2.8 Current distribution along the half-wave dipole at scale = 5

From figures 2.5-2.8, it is obvious that, the current distribution becomes smoother with higher scale. That means, higher scales correspond to detailed information of the function whereas lower scales correspond to non-detailed information of the function.

The comparison of total CPU time for complete analysis of the current distribution along the half-wave dipole for semi-orthogonal wavelets has given below -

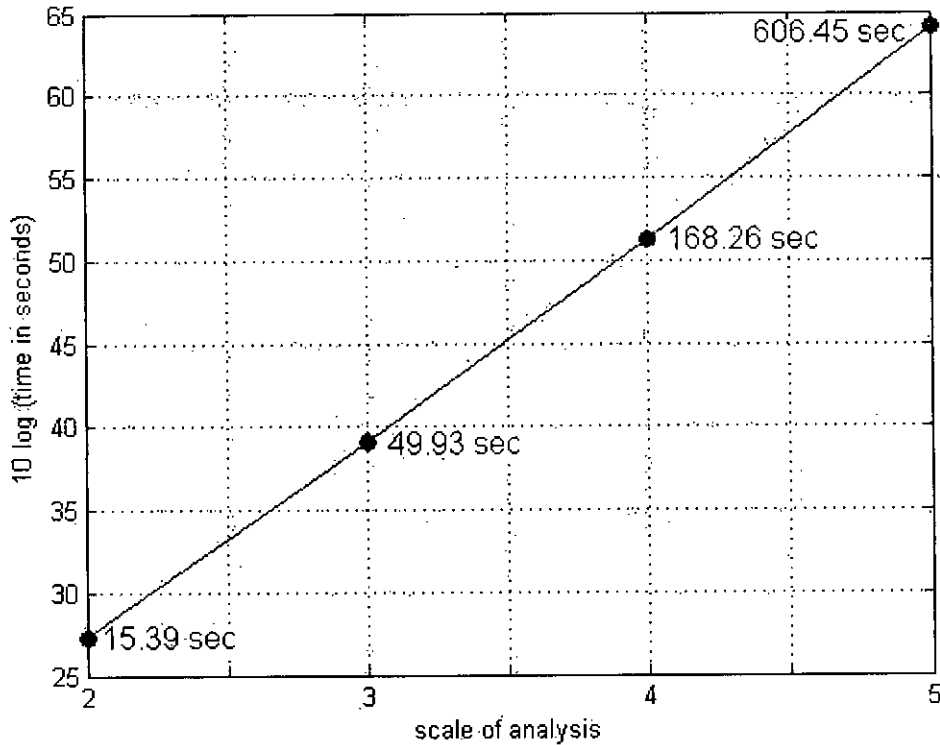


Fig. 2.9 CPU time for complete analysis of half-wave dipole at different scales

From figure 2.9 it is found that – the computing time increases logarithmically with respect to the scale of analysis. So, efficient scale should be chosen with optimum level of information and computing time. From the previous observations, it can be said that – for the current distribution analysis of a half-wave dipole, scale = 3 is the most efficient with respect to both function details and time requirement.

### 2.3 Current Distribution of a Receiving Half-wave Dipole Antenna

Current distribution along the length of a half-wave receiving dipole antenna operated at the same frequency (300MHz), with same length and radius has been calculated at different scale and the results are shown in the following figure.

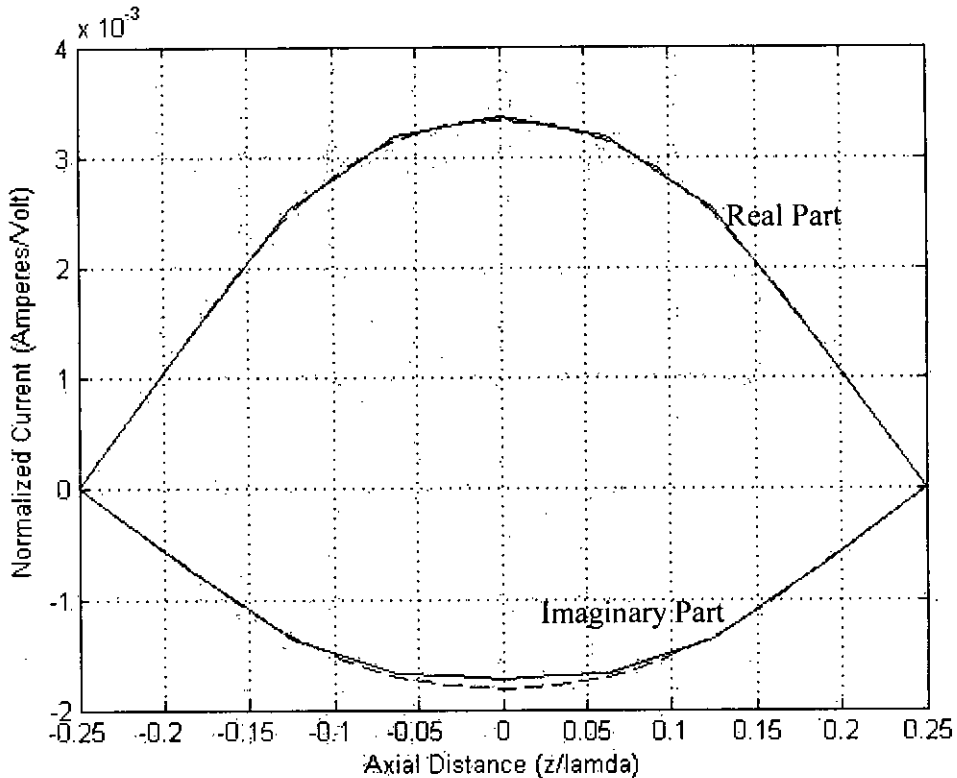
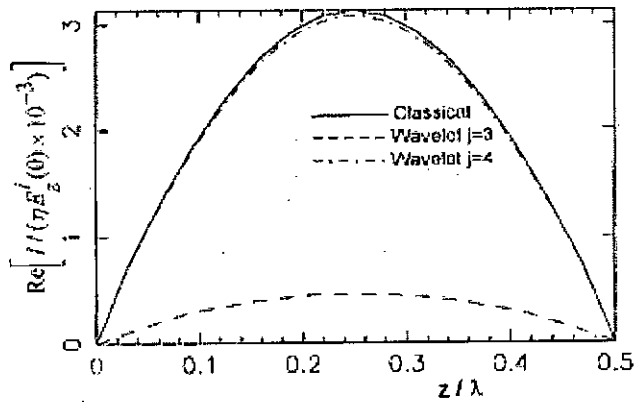


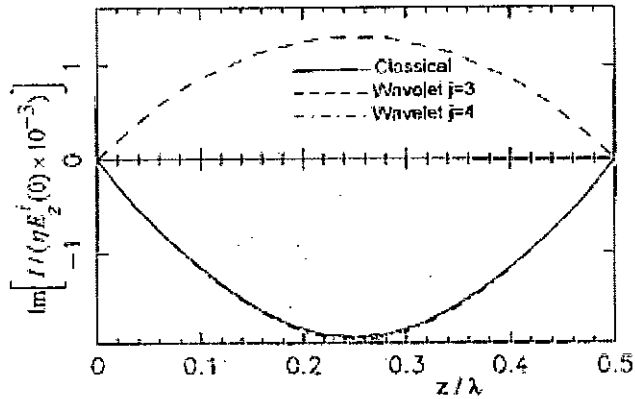
Fig. 2.10 Current distributions along the half-wave receiving dipole at scale = 2 & 3

From the figure 2.10 it is observed that, the current distribution function does not vary with scale, since it is very difficult to distinguish the results. From the previous discussion for half-wave transmitting dipole operated at the same frequency and with the same antenna length and radius, it can be said that – higher scale contains details function information; except this there is no difference in phase and magnitude between the results.

Nevels, Goswami and Tehrani [17] used semi-orthogonal spline wavelets and they analyzed the current distribution along a half-wave receiving dipole. The analyzed result has been compared with their result in the next page.



(a)



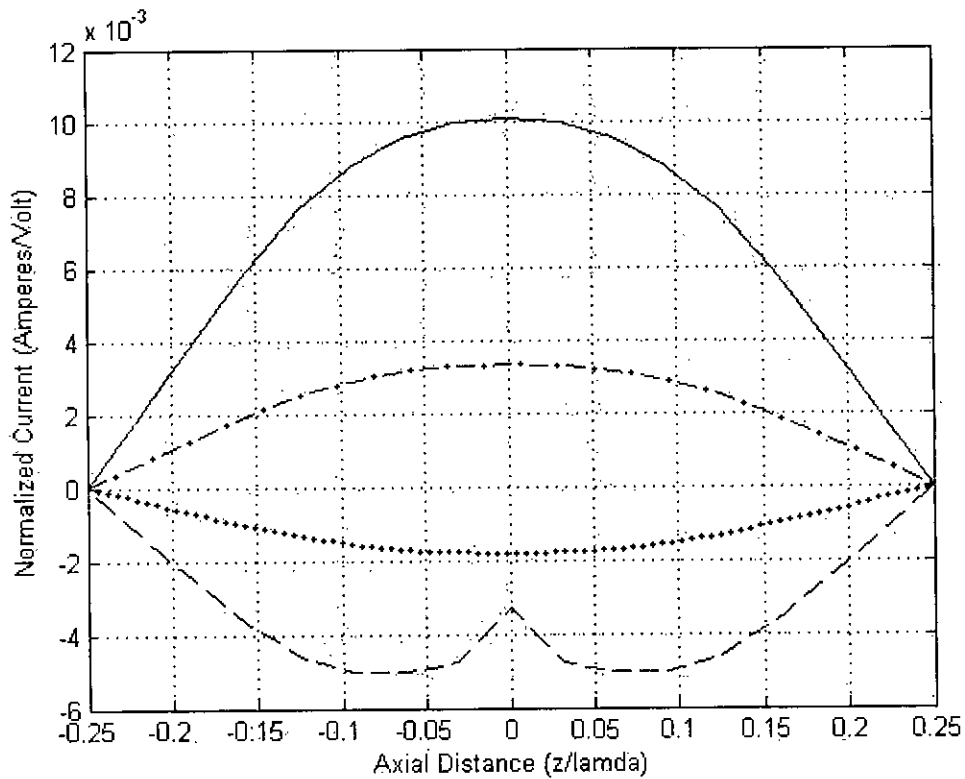
(b)

Fig. 5. (a) The real and (b) imaginary parts of the current on a thin wire scatterer computed using spline semi-orthogonal scaling functions and wavelets at the single octave levels  $j = 3$  and  $j = 4$  compared with the classical triangular basis function current.

Fig. 2.11 Current distributions for half-wave receiving dipole at scale = 3 & 4 by Nevels

From the figure 2.11 it is clear that – the result at scale = 3 is not the true current distribution along the antenna. Significant result was obtained at scale = 4. But in our analysis we have obtained the proper result at the lowest scale, i.e. scale = 2. With respect to this, it can be said that – our approach is superior to them. To reduce the computing time, they applied threshold technique to make the matrix sparse. But in our analysis we have found that – threshold is not required at all, since the matrix equation can be solved within few milliseconds (generally within 75 ms); when the total computation time is spent to find out the matrix elements.





———— :TxReal; - - - - - :TxImag.; - · - · - :RxReal; ..... :RxImag.

Fig. 2.12 Comparison of transmitting (Tx) and a receiving (Rx) half-wave dipole current

If the current distribution along a center-fed transmitting half-wave dipole and a receiving half-wave dipole of the same length and operating frequency will be compared, noticeable difference in imaginary part of current distribution is found at center of the antenna length. In case of receiving antenna, the imaginary part of current distribution is maximum at the center of the antenna; when for transmitting antenna the current reaches at peak outside the centered delta-gap. The difference is obtained due to the difference in E-field that has considered in the analysis. For receiving antenna the current induced by a plane wave incident from broadside. i.e. the antenna experienced a constant E-field along its length. On the other hand, for transmitting antenna the induced E-field exists only in the delta-gap.

## 2.4 Comparison with Mack's and King's Values for Half-wave Dipole

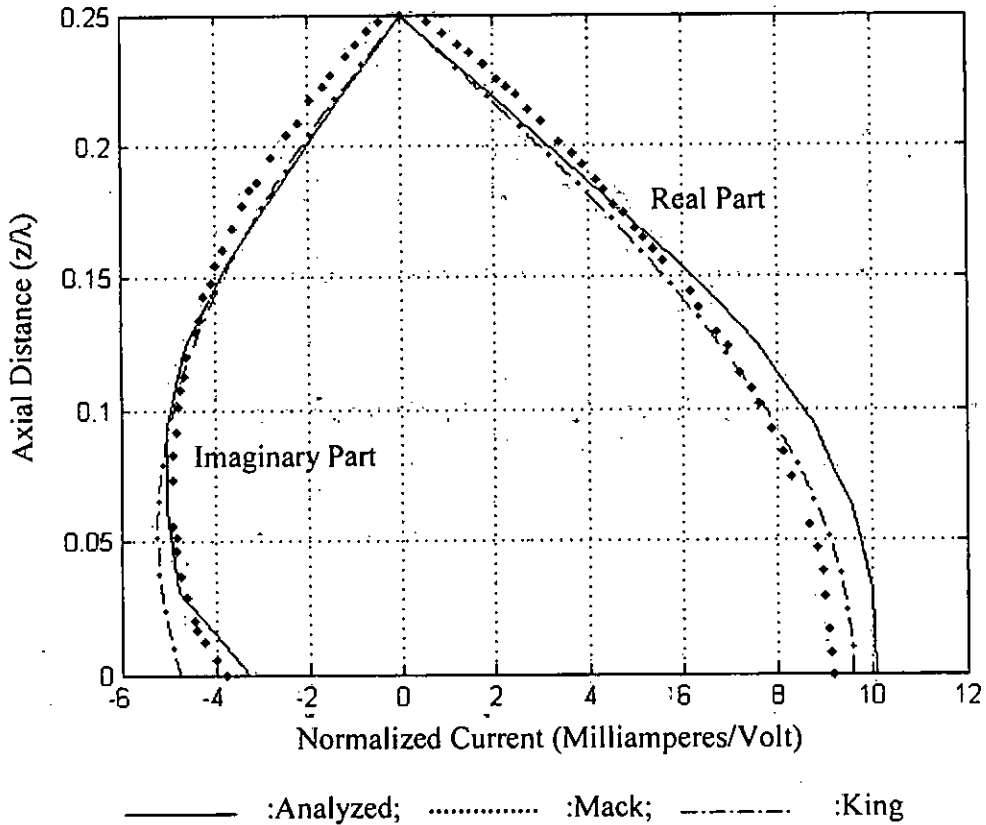


Fig. 2.13 Comparison of current distributions for the half-wave dipole at scale = 3

In figure 2.13, analyzed current distribution is compared with the measured values of Mack and the theoretical current distribution as per King's Three-term approximation. Relative error of the result with Mack's measurement is 10.59% for real part and 9.55% for imaginary part, when with respect to King's approximation the error is 8.42% and 11.22% respectively. Relative error for King's distribution with Mack's values is found 6.98% for real part and 11.37% for imaginary part. Therefore, accuracy of the analyzed result is comparatively acceptable.

## 2.5 Current Distribution of a Full-wave Transmitting Dipole

Current distribution along the length of a full-wave transmitting dipole antenna (i.e.  $k_0 h = \pi$ , where  $h$  = half-length of antenna) operated at the same frequency (300MHz), driven by the same EMF ( $V_0 = 1$  volt) and with same antenna radius ( $a = 7.022 \times 10^{-3} \lambda = \Delta z$ ) has been calculated at different scale and the results are shown in the following figure.

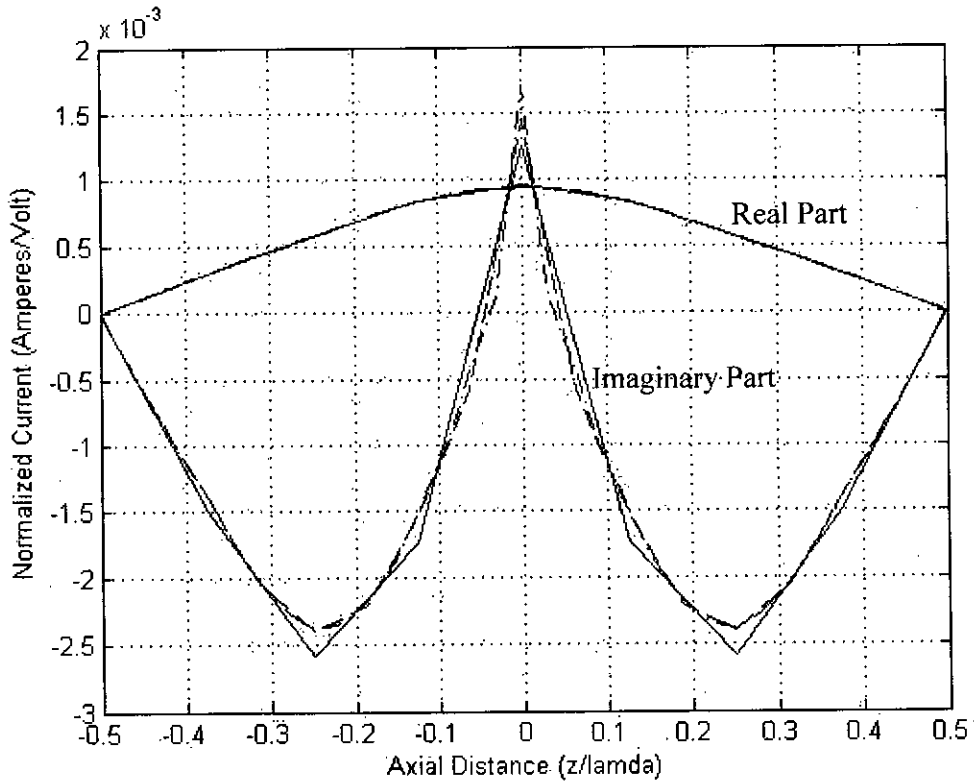


Fig. 2.14 Current distributions along the full-wave transmitting dipole at different scales

Current distributions along the full-wave dipole at different scale are shown in figure 2.14. But, the results are too close to distinguish the variation with respect to different scales. So in next page, results at each scale have been provided for better understanding.

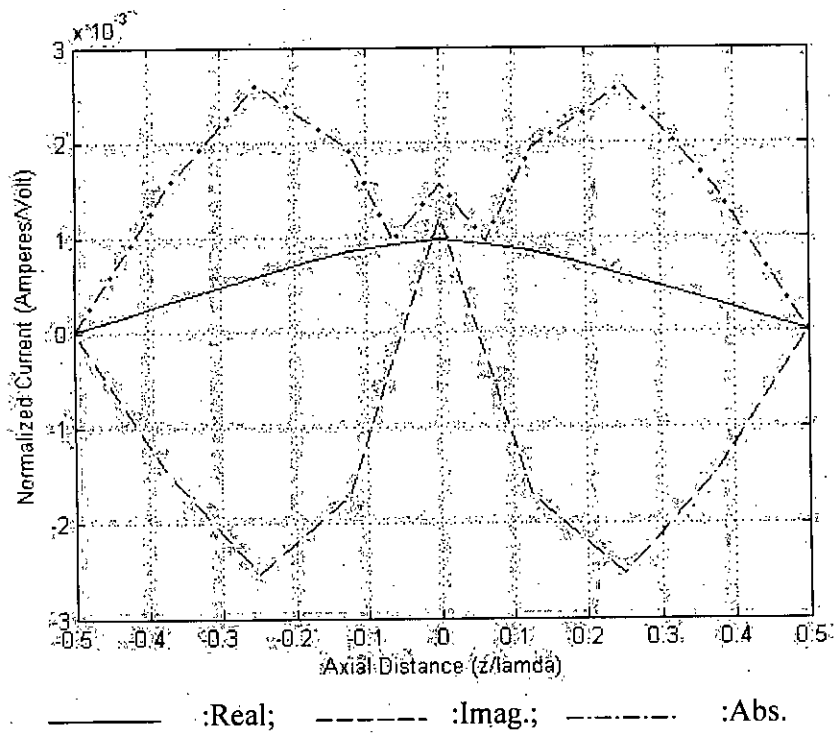


Fig. 2.15 Current distribution along the full-wave dipole at scale = 2

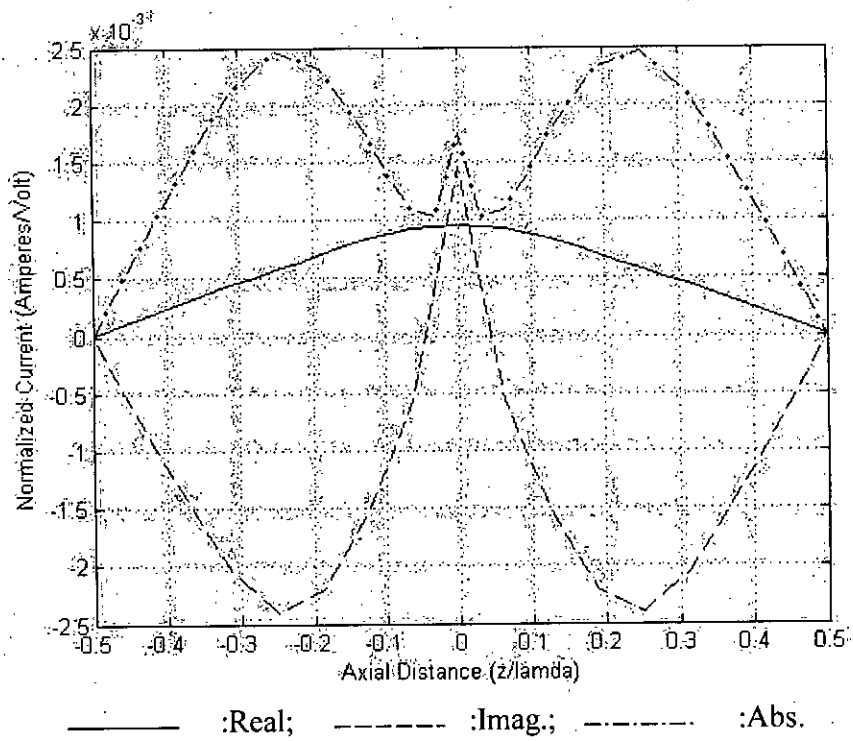


Fig. 2.16 Current distribution along the full-wave dipole at scale = 3

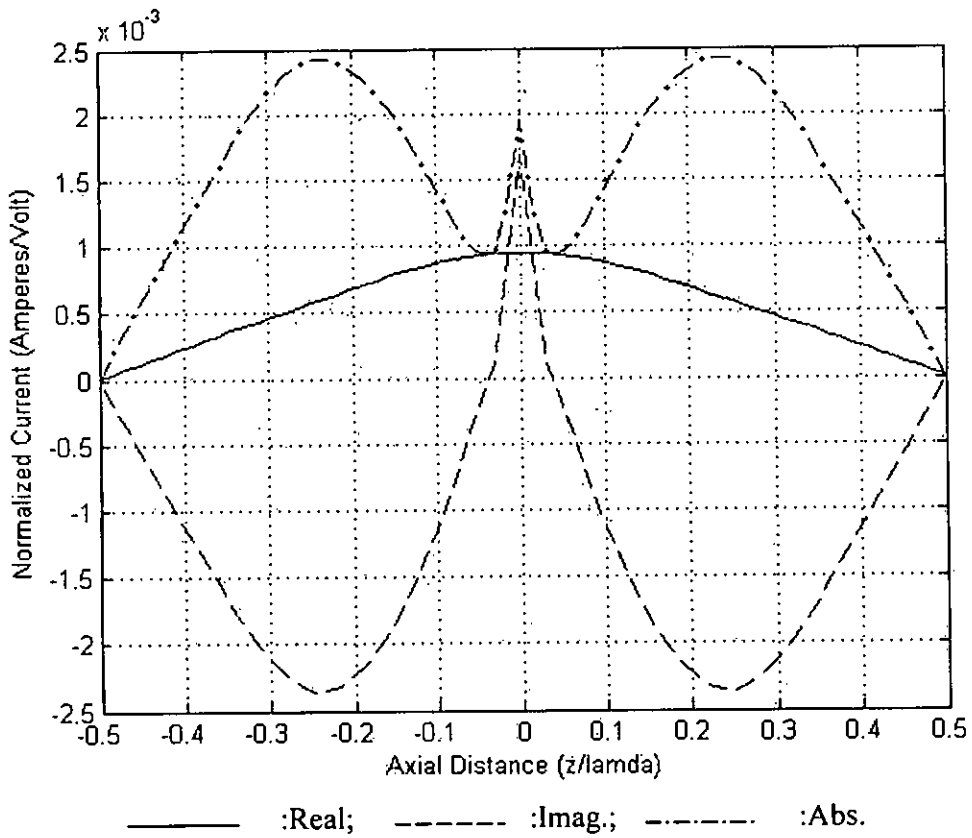


Fig. 2.17 Current distribution along the full-wave dipole at scale = 4

From figures 2.15-2.17, it is obvious that, the current distribution becomes smoother with higher scale. That means higher scales correspond to detailed information of the function whereas lower scales correspond to non-detailed information of the function.

The comparison of total CPU time for complete analysis of the current distribution along the full-wave dipole for semi-orthogonal wavelets has given below -

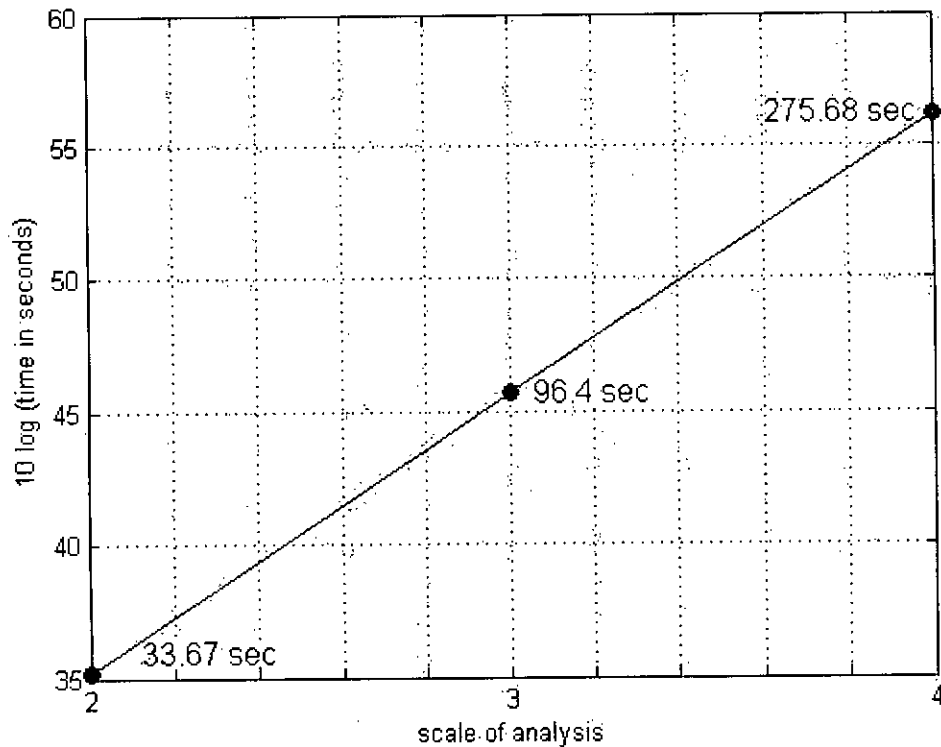


Fig. 2.18 CPU time for complete analysis of full-wave dipole at different scales

From figure 2.18 it is found that – the computing time increases logarithmically with respect to the scale of analysis. So, efficient scale should be chosen with optimum level of information and computing time. From the previous observations, it can be said that – for the analysis of a full-wave dipole current distribution, scale = 4 is the proper scale which gives the optimum information with optimum computation time.

## 2.6 Comparison with Mack's and King's Values for Full-wave Dipole

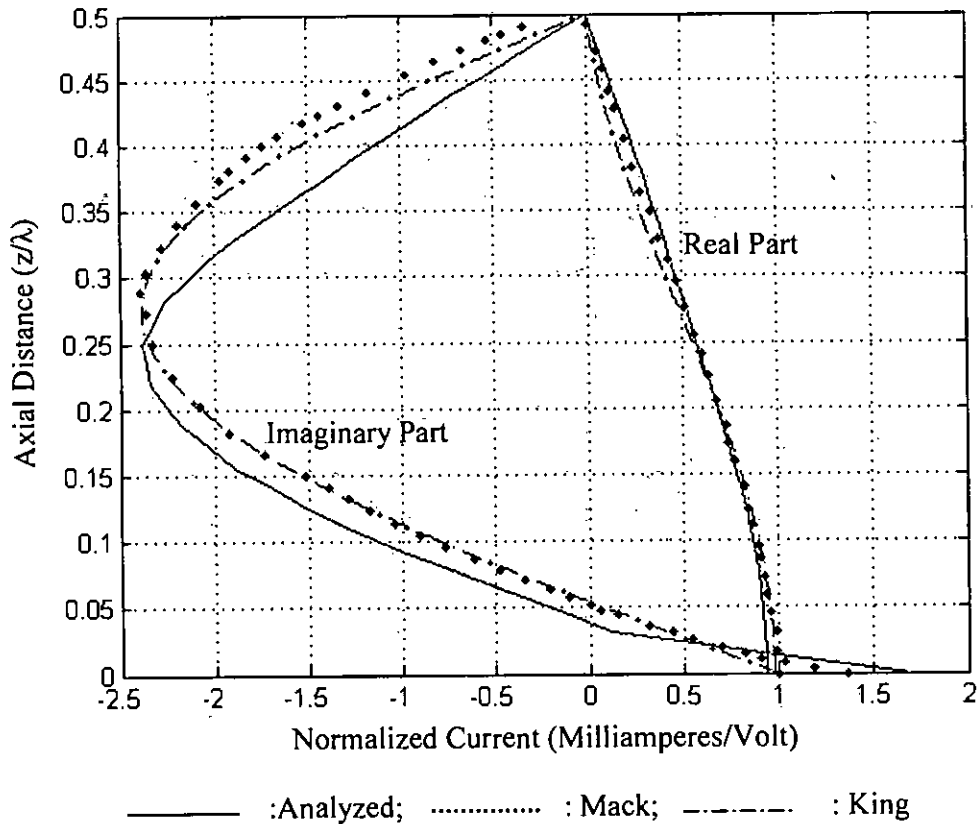


Fig. 2.19 Comparison of current distributions for a full-wave dipole at scale = 4

In figure 2.19, analyzed current distribution is compared with the measured values of Mack and the theoretical current distribution as per King's Three-term approximation. Relative error of the result with Mack's measurement is 4.12% for real part and 24.89% for imaginary part, when with respect to King's approximation the error is 7.12% and 23.57% respectively. Relative error for King's distribution with Mack's values is found 4.28% for real part and 9.48% for imaginary part. Imaginary part of the analyzed result deviate much from Mack's measured result for  $z/\lambda = 0.25$  to  $0.5$ . Though the error is much higher than King's, it follows the measured data comparatively better for  $z/\lambda = 0$  to  $0.25$ . Therefore, accuracy of the analyzed result is relatively acceptable.

## 2.7 Discussion

From the analysis it is found that – the most efficient scale is three, for current distribution analysis along a half-wave dipole and along a full-wave dipole it is four. The accuracy of the result is also acceptable comparing to Mack's measured value and King's Three-term approximation. It is also observed that – with respect to computation time, this method is faster to analyze electrically short antennas; for electrically large structure it takes higher computation time. In our analysis we have taken the operating frequency as 300 MHz and corresponding antenna length for half-wave dipole is 0.5 meter and 1 meter for full-wave dipole. But practically, it should be 0.475 meter and 0.95 meter respectively; as the velocity of the wave along the antenna is slower than that in free space. In fact, for most antennas the velocity is 95% of 'c'. We have also considered zero current at the ends of the finite length wire, which is the usual practice when enforcing the boundary condition. If it is not considered, boundary wavelets and scaling functions should also be included in calculation; which will ultimately increase the computation time further. Enforcing zero current at the antenna end can be explained by visualizing the current flow in the antenna. For example, if the frequency of the voltage source is increased so that the wavelength is approximately equal to or less than the length of the wire, the current points in different directions at different locations of the antenna. These opposing currents cause destructive interference and will appear to be a standing wave. The maximum current will be seen at the center of the wire and no current will be at the ends. This occurs because the electrons flowing out to the ends reflect back toward the center where they meet the next wave and the current is reinforced there.



## **CHAPTER – 3**

### **CURRENT DISTRIBUTION OF A WIRE IN A YAGI-UDA ARRAY**

### 3.1 General Formulation

For an arbitrary array of parallel linear antennas the current distribution on each antenna will be effected by mutual couplings between the antennas. In the case of  $N$  parallel dipoles in side-by-side arrangement with centers at position  $(x_n, y_n)$ , and driving voltages, lengths and radii  $V_n, l_n, a_n$  where  $n = 1, 2, \dots, N$ ; the magnetic vector potential of the antenna array with respect to an observation point  $(x, y, z)$  is given as [20].

$$\vec{A}(\vec{r}) = \hat{z} \frac{\mu}{4\pi} \sum_{n=1}^{n=N} \left( \int_{-l_n/2}^{l_n/2} I_{z_n}(z') \frac{e^{-jk\sqrt{(z-z')^2 + (x-x_n)^2 + (y-y_n)^2}}}{\sqrt{(z-z')^2 + (x-x_n)^2 + (y-y_n)^2}} dz' \right) \quad (3.1.1)$$

Let us consider a Yagi-Uda array of three  $z$ -directed parallel dipoles with centers at locations  $(0, 0, 0)$ ,  $(0, d_{12}, 0)$  and  $(0, d_{13} = d_{12} + d_{23}, 0)$  as shown in Fig. 3.1. The second or active dipole is center-driven by a voltage generator  $V_2$  and the other two dipoles, i.e. reflector and director are parasitic. Let  $I_1(z)$ ,  $I_2(z)$  and  $I_3(z)$  are the currents induced on the dipoles;  $l_1, l_2$  and  $l_3$  are the antenna lengths;  $a_1, a_2, a_3$  are their radii respectively.

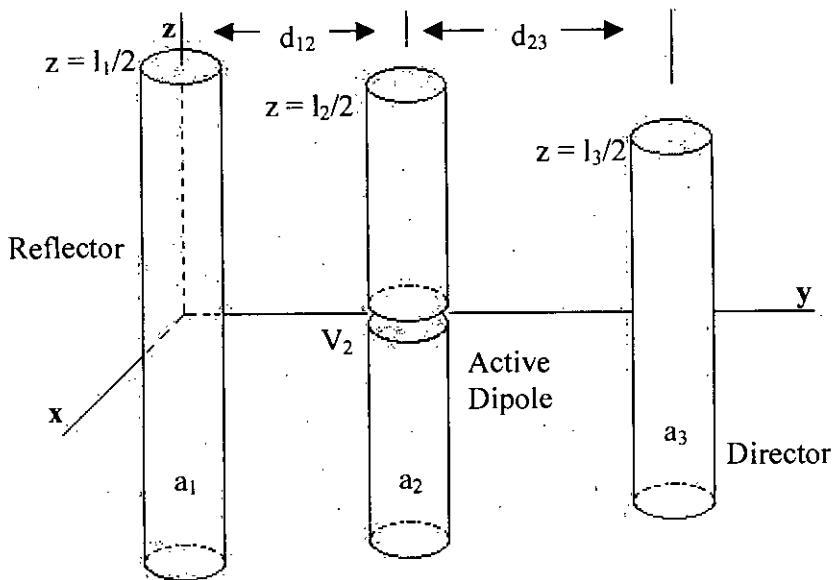


Fig. 3.1 Three-element Yagi-Uda array

Therefore, the Pocklington's integral equation for the m-th antenna can be generalized into –

$$\frac{j\eta\lambda}{8\pi^2} \left( \frac{\partial^2}{\partial z^2} + k^2 \right) \sum_{n=1}^{n=N} \left( \int_{-l_n/2}^{l_n/2} I_{z_n}(z') \frac{e^{-jk\sqrt{(z-z')^2 + d_{mn}^2}}}{\sqrt{(z-z')^2 + d_{mn}^2}} dz' \right) = E_{z_n}^{in}(z) \quad (3.1.2)$$

$$\text{where, } d_{mn} = \begin{cases} y_m - y_n; & \text{when } m \neq n \\ a_n; & \text{when } m = n \end{cases}$$

$$\text{and } E_{zn}^{in}(z) = \begin{cases} 0; & \text{for } n = 1, 3. \\ V_2 / \Delta z; & \text{for } n = 2 \end{cases}$$

The unknown current function  $I_{zn}(z')$  of each antenna can be expanded using semi-orthogonal wavelets. Applying Galerkin's technique for the respective antenna's basis function in respective antenna equation and solving the impedance matrix, the current distribution on each antenna can be derived.

### 3.2 Current Distributions of a Three-element Yagi-Uda Array

Let us consider an Yagi-Uda array operating at 300MHz, has a reflector, an active dipole and one director of length,  $l_r = 0.51\lambda$ ,  $l_a = 0.5\lambda$  and  $l_d = 0.4\lambda$  respectively and radius of each element is  $0.00337\lambda$ . The spacing between reflector and active dipole is  $0.25\lambda$  and between director and active dipole is  $0.3\lambda$ .

Now applying the semi-orthogonal wavelets as basis the current function can be constructed at different scale. As the dipoles are approximately equal to the half-wave dipole, we have analyzed the current distribution at scale = 3. The results have been shown in next pages.

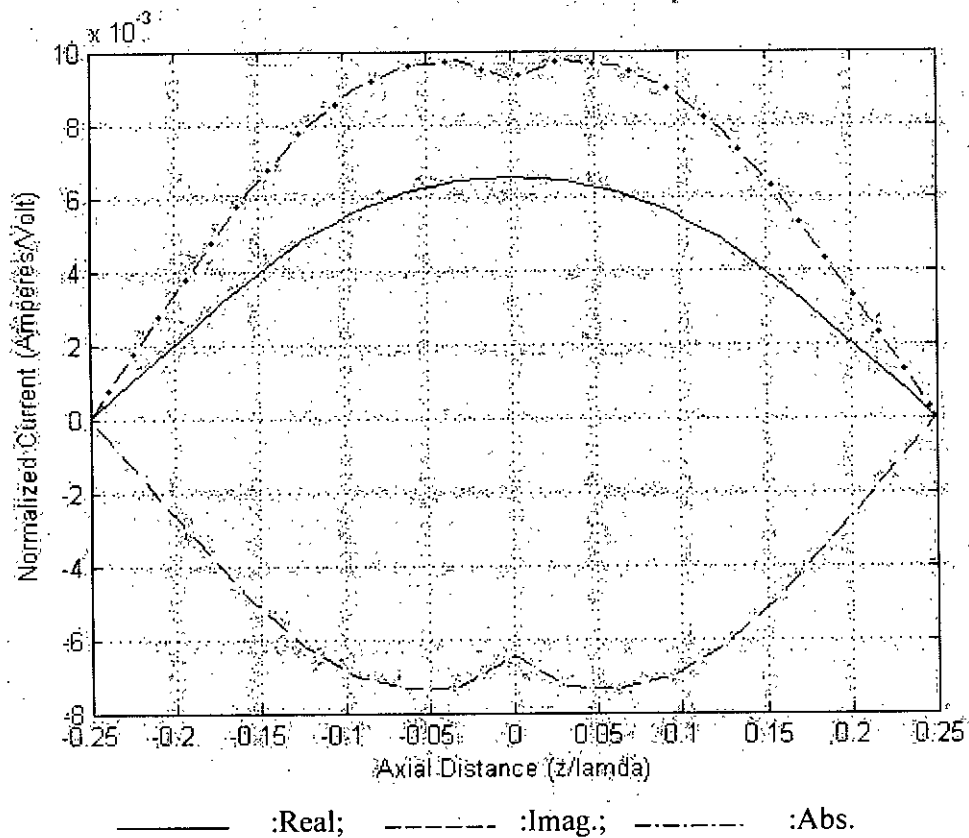


Fig. 3.2 Current distribution along the active dipole at scale = 3

The figure shows the current distribution along the active dipole of the three-element Yagi-Uda array. From the analyzed current distribution it is noted that – the magnitude of the current has been reduced for real part, but increased for imaginary part with respect to single half-wave transmitting dipole of the same. That means at Yagi-Uda arrangement the mutual coupling between the antenna plays significant impact on each antenna characteristic.

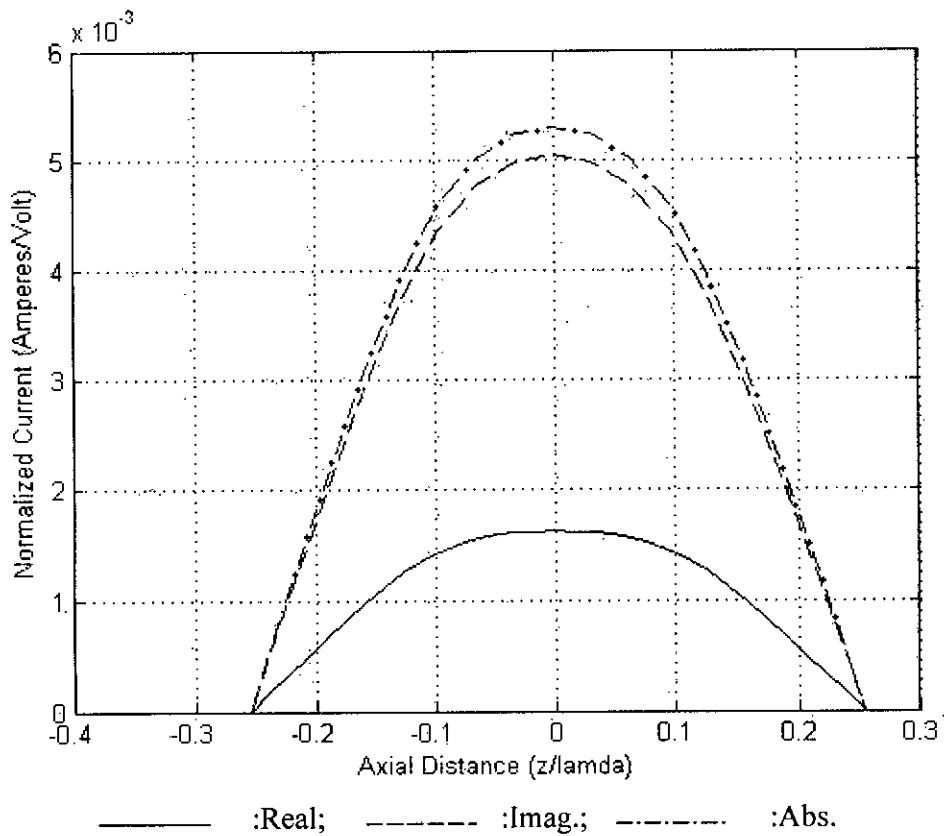


Fig. 3.3 Current distribution along the reflector at scale = 3

The figure shows the current distribution along the reflector element of the three-element Yagi-Uda array. From the analyzed current distribution it is found that – both the real and imaginary part of the current exists in the same side, i.e. has positive values. The magnitude of the real part is comparatively less than that of imaginary.

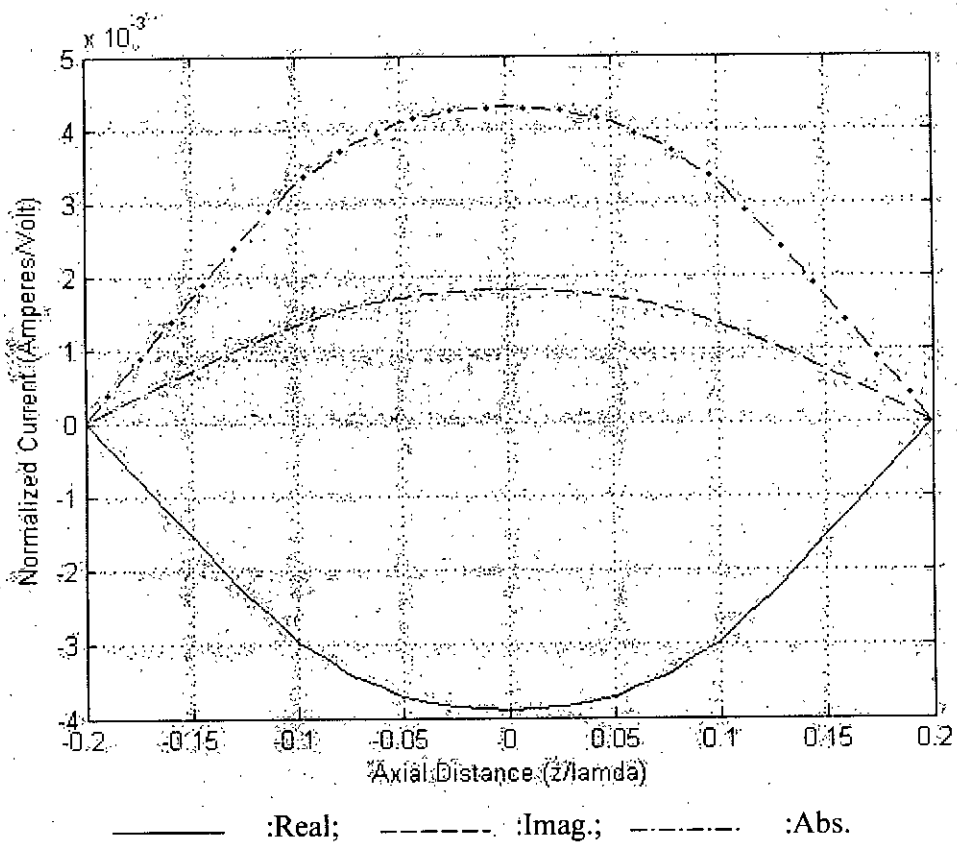
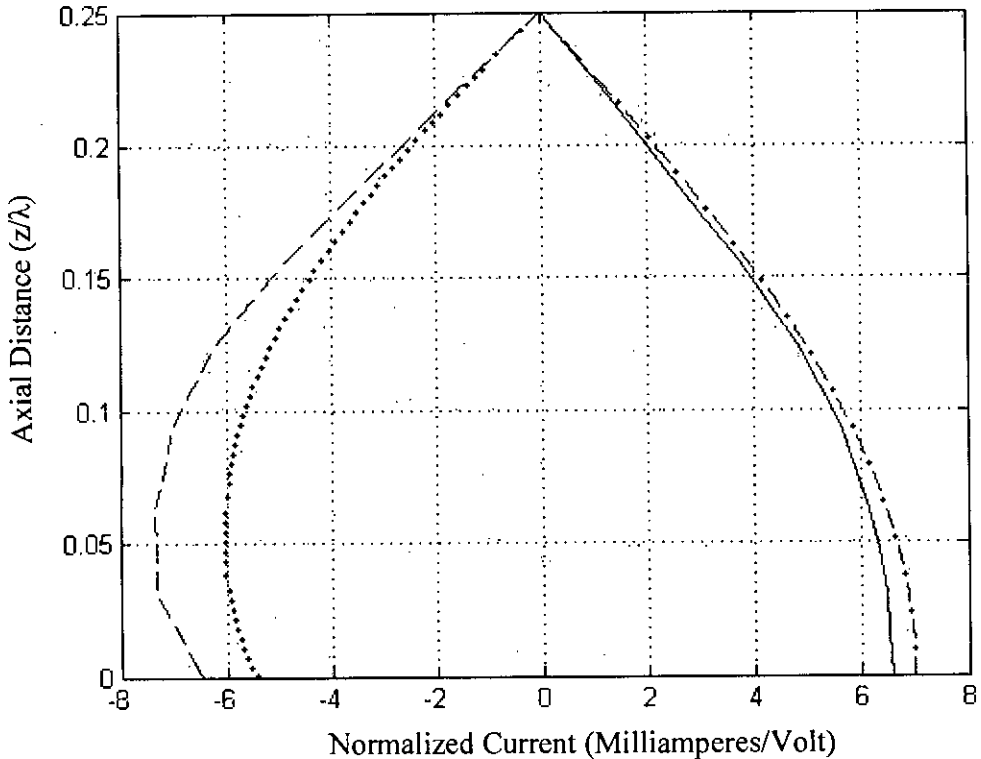


Fig. 3.4 Current distribution along the director at scale = 3

The figure shows the current distribution along the director element of the three-element Yagi-Uda array. From the analyzed current distribution it is found that – the current is totally out of phase with respect to the active dipole current. Moreover, the magnitude of the real part is comparatively higher than that of imaginary.

### 3.3 Comparison with King's Three-term Approximation

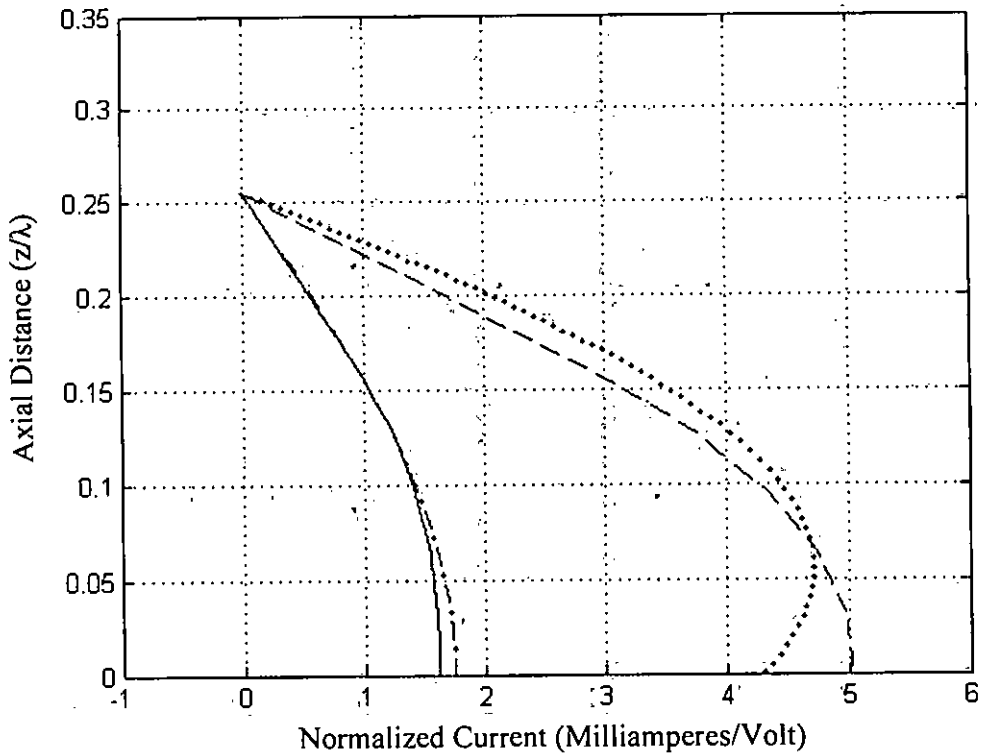
Analyzed current distribution along each antenna element of the three-element Yagi-Uda array has been compared with the King's Three-term approximation for a ten-element Yagi-Uda array [21] to check the accuracy level.



———— :AnzReal;    - - - - - :AnzImag;    - · - · - · :KingReal;    ········· :KingImag.

Fig. 3.5 Comparison of current distributions for the active dipole at scale = 3

Figure 3.5 shows the comparison between analyzed current distribution and King's result for active dipole of the three-element array. Relative error between the results is 5.28% for real part and 19.95% for imaginary part. Real part is much closer to King's approximation than imaginary part of the current. The imaginary part differs significantly because King's approximation was for ten-element array rather than three as analyzed here.

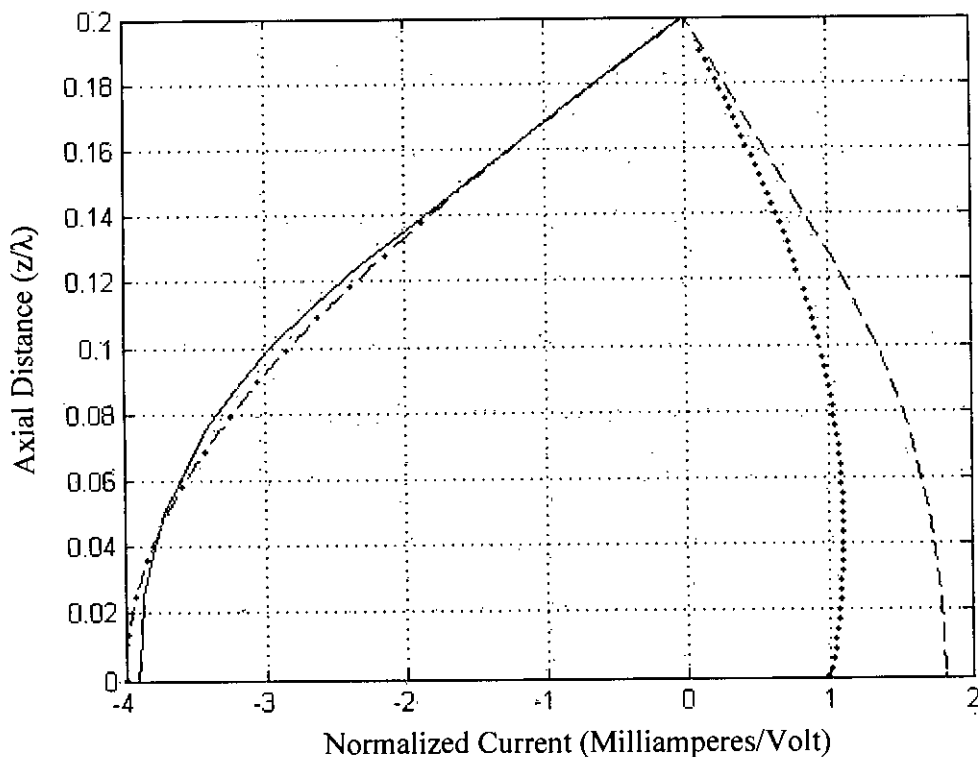


———— :AnzReal; - - - - - :AnzImag.; - · - · - · :KingReal; ..... :KingImag.

Fig. 3.6 Comparison of current distributions for the reflector at scale = 3

Figure 3.6 shows the comparison between analyzed current distribution and King's result for reflector element of the three-element array. Relative error between the results is 4.94% for real part and 9.28% for imaginary part. Real part is much closer to King's approximation than imaginary part of the current.





———— :AnzReal;    - - - - - :AnzImag.;    - · - · - · :KingReal;    ..... :KingImag.

Fig. 3.7 Comparison of current distributions for the director at scale = 3

Figure 3.7 shows the comparison between analyzed current distribution and King's result for active dipole of the three-element array. Relative error between the results is 2.63% for real part and 55.47% for imaginary part. Result is too close for real part but differs significantly for imaginary part of the current. Result has been compared with ten-element array, which has eight directors. But the analyzed array has only one director.

### 3.4 Discussion

To calculate the current distributions on each element of the Yagi-Uda array, it has taken total 534.587 seconds at scale = 3 (for scale = 2 it has taken 150.35 seconds). We compared the result at scale = 3, since the function information is optimum at this scale. From the comparison it has been verified that the current distribution is close to the theoretical estimation in most cases, though the estimation is for a ten-element Yagi-Uda array.

## **CHAPTER – 4**

### **INPUT IMPEDANCE OF THE WIRE ANTENNA**

#### 4.1 General Formulation

The input impedance of a linear wire antenna can be calculated by evaluating the n field on the surface of the antenna. Hence, the impedance is –

$$Z = -\frac{1}{|I(0)|^2} \int_{-l/2}^{l/2} E(z) I(z) dz \quad (4.1.1)$$

For a transmitting antenna –

$$\begin{aligned} E(z) &= -V_0/\Delta z \quad ; \quad -\Delta z/2 \leq z \leq \Delta z/2 \\ &= 0 \quad ; \quad \text{elsewhere} \end{aligned} \quad (4.1.2)$$

If  $V_0 = 1$  volt and  $\Delta z = a$  then –

$$Z = \frac{1}{a|I(0)|^2} \int_{-a/2}^{a/2} I(z) dz = \frac{1}{I(0)}, \text{ when } I(-a/2) = I(a/2) = I(0) \quad (4.1.3)$$

#### 4.2 Impedance of the Linear Wire Antenna and Array

The calculated input impedance of the half-wave dipole is  $(90.0667 + j 29.0237) \Omega$ ; where according to King's Three-term approximation it is  $(83.3333 + j 41.6667) \Omega$  and as per Mack's measurement it is  $(94.6746 + j 39.4477) \Omega$ .

For full-wave dipole, the calculated input impedance is  $(251.8 - j 449.99) \Omega$ ; where according to King's Three-term approximation and Mack's measurement it is  $(506.04 - j 512.26) \Omega$  and  $(337.84 - j 472.97) \Omega$  respectively.

The input impedance of the three-element Yagi-Uda array is found  $(77.2734 + j 76.1564) \Omega$ ; when as per King's Three-term approximation for ten-element array it is  $(88.3281 + j 69.4) \Omega$ .

#### 4.3 Discussion

The input impedance of a straight wire antenna has been calculated using the current distribution obtained in Chapter –2 and Chapter –3. The results have been compared with those obtained by King's Three-term approximation and with the measured values reported by Mack. In case of half-wave dipole, the analyzed resistance is lower than measured value but higher than theoretical value; when the reactance is lower from both reactances. For full-wave dipole, both the resistance and reactance is lower. In case of three-element Yagi-Uda array the result is lower for resistance but higher in reactance compared to theoretical value for ten-element array. It is noted that – antenna impedance varies with the antenna arrangement. Input impedance of the same half-wave dipole has been reduced in resistance and increased in reactance in presence of other parasitic elements. This represents – for specific arrangement of antenna array, the power stored in the near field increases; when the power associated with radiation and dielectric & conducting losses reduces.

## **CHAPTER – 5**

### **FAR-FIELD RADIATION PATTERN OF THE WIRE ANTENNA**

## 5.1 General Formulation

At far-field condition ( $r \gg 2l^2/\lambda$ ) the magnetic vector potential of a z – directed linear antenna can be approximated as –

$$\vec{A}(\hat{r}) = \hat{z} \frac{\mu e^{-jkr}}{4\pi r} F_z \quad (5.1.1)$$

where,  $\vec{F} = \hat{z} F_z = \hat{r} \cos\theta F_z - \hat{\theta} \sin\theta F_z$  is known as the radiation vector.

For a single linear antenna –

$$F_z = \int_{-l/2}^{l/2} I(z') e^{jk \cos\theta z'} dz' \quad (5.1.2)$$

For an array of linear antennas along y – axis the radiation vector is –

$$F_z = \sum_{n=1}^{n=N} e^{jk \sin\theta \sin\phi y_n} \left( \int_{-l_n/2}^{l_n/2} I_n(z') e^{jk \cos\theta z'} dz' \right) \quad (5.1.3)$$

In terms of the radiation vector  $F_z(\theta, \phi)$ , the radiation intensity of the linear wire antenna becomes –

$$U(\theta, \phi) = \frac{\eta k^2}{32\pi^2} |\vec{F}(\theta, \phi)|^2 = \frac{\eta k^2}{32\pi^2} |\sin\theta F_z|^2 \quad (5.1.4)$$

and the normalized power gain is –

$$g(\theta, \phi) = \frac{U(\theta, \phi)}{U_{\max}} \quad (5.1.5)$$

## 5.2 Far-field Radiation Pattern for the Linear Wire Antenna

From the basic definition of integral formula we have –

$$\int_a^b f(x) dx = \lim_{n \rightarrow \infty} \sum_{k=1}^{k=n} f(x_k^*) \Delta x \quad (5.2.1)$$

where,  $\Delta x = \frac{b-a}{n}$  and  $x_k = a + k \Delta x$ ; when  $x_k^* \in [x_{k-1}, x_k]$

Now, for the linear wire antenna the radiation vector  $|\vec{F}(\theta, \phi)| = |\sin \theta F_z(\theta)|$ . Hence, using this definition of equation (5.2.1) in equation (5.1.4) we have –

$$U(\theta, \phi) = \frac{\eta k^2}{32\pi^2} |\sin \theta F_z(\theta)|^2 \quad (5.2.2)$$

$U(\theta, \phi)$  will be maximum at  $\theta = \pi/2$ . Therefore, as per equation (5.1.5) the normalized power gain can be expressed as –

$$g(\theta, \phi) = \left[ \frac{\sin \theta \left( \sum_{m=1}^{m=n} I(z'_m) e^{j k \cos \theta (z'_m)} \right)}{\left( \sum_{m=1}^{m=n} I(z'_m) \right)} \right]^2 \quad (5.2.3)$$

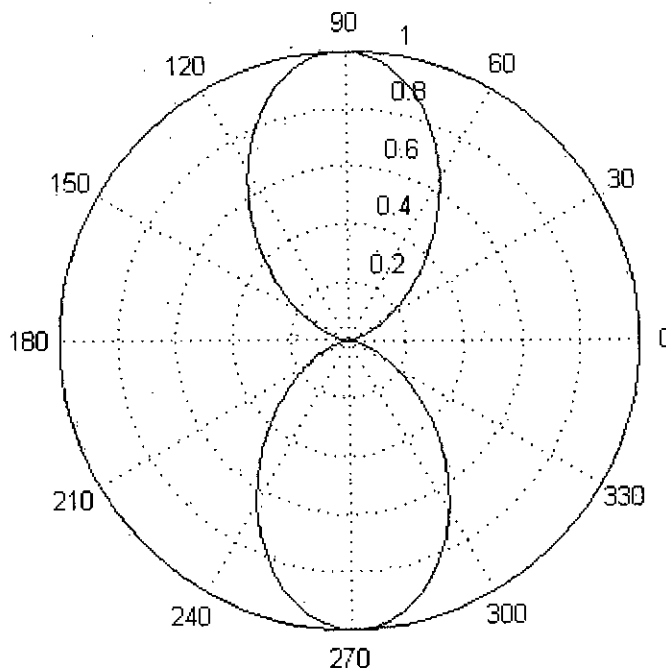


Fig. 5.1 Azimuthal pattern [polar plot of  $g(\theta, \phi)$ ] of the half-wave dipole in absolute units

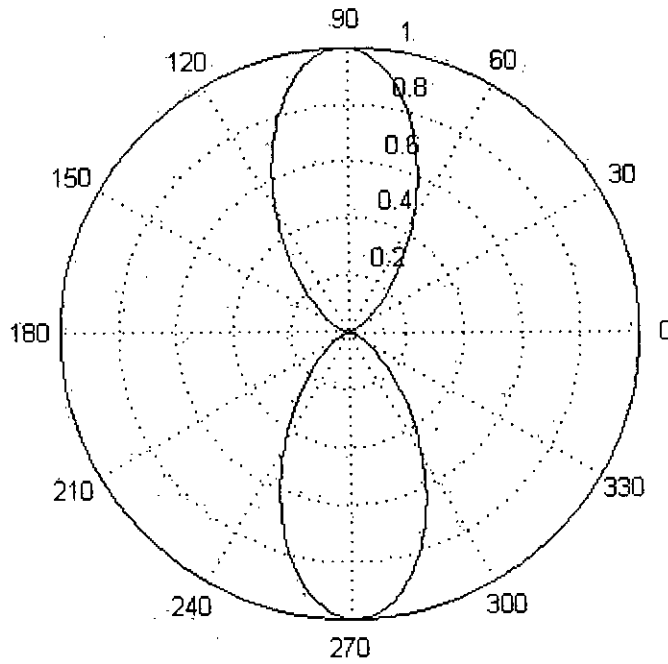


Fig. 5.2 Azimuthal pattern [polar plot of  $g(\theta, \phi)$ ] of the full-wave dipole in absolute units

### 5.3 Far-field Radiation Pattern for the Antenna Array

For the discussed three-element Yagi-Uda array –

$$\begin{aligned}
 F_z(\theta, \phi) = & \int_{-l_1/2}^{l_1/2} I_1(z') e^{j k \cos \theta z'} dz' + e^{j k \sin \theta \sin \phi d_{12}} \int_{-l_2/2}^{l_2/2} I_2(z') e^{j k \cos \theta z'} dz' \\
 & + e^{j k \sin \theta \sin \phi d_{13}} \int_{-l_3/2}^{l_3/2} I_3(z') e^{j k \cos \theta z'} dz' \quad (5.3.1)
 \end{aligned}$$

$$\begin{aligned}
 = & \left[ \sum_{m=1}^{m=n} I_1(z'_{m1}) e^{j k \cos \theta (z'_{m1})} \right] \Delta z'_1 \\
 & + \left[ \sum_{m=1}^{m=n} I_2(z'_{m2}) e^{j k [\cos \theta (z'_{m2}) + \sin \theta \sin \phi d_{12}]} \right] \Delta z'_2 \quad (5.3.2) \\
 & + \left[ \sum_{m=1}^{m=n} I_3(z'_{m3}) e^{j k [\cos \theta (z'_{m3}) + \sin \theta \sin \phi d_{13}]} \right] \Delta z'_3
 \end{aligned}$$

$U(\theta, \phi)$  will be maximum at  $\theta = \pi/2$  for azimuthal or E-plane pattern and at  $\phi = \pi/2$  for H-plane pattern.

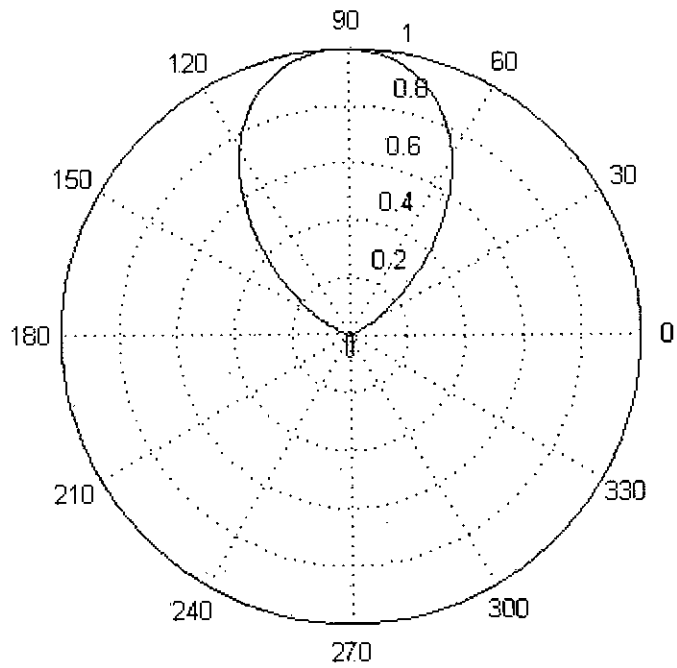


Fig. 5.3 E-plane pattern [polar plot of  $g(\theta, \phi)$ ] of the Yagi-Uda array in absolute units

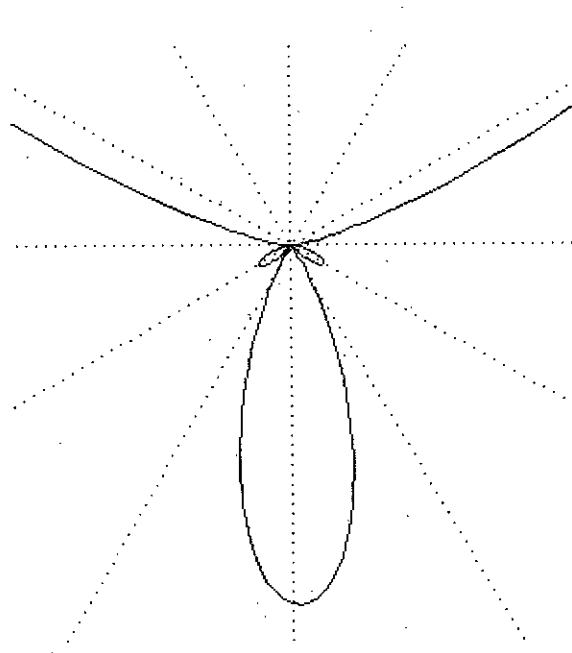


Fig. 5.4 Magnified rear view of the E-plane pattern of the Yagi-Uda array



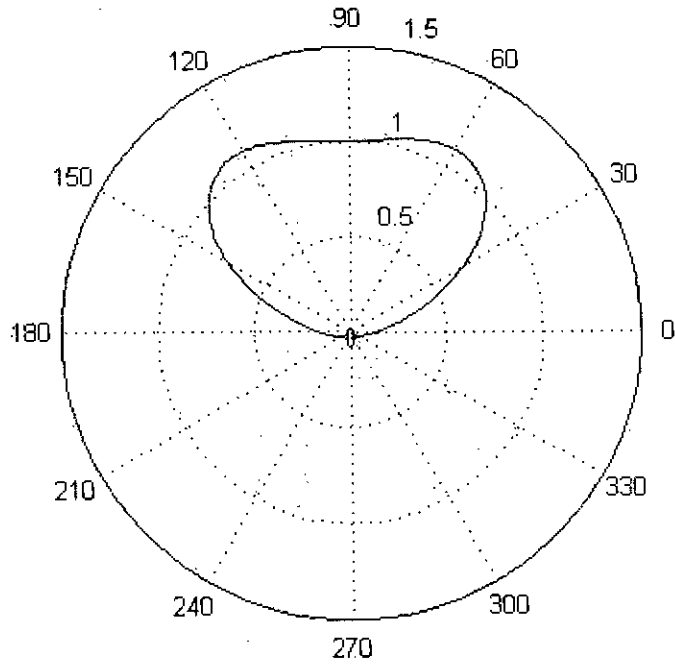


Fig. 5.5 H-plane pattern [polar plot of  $g(\theta, \phi)$ ] of the Yagi-Uda array in absolute units

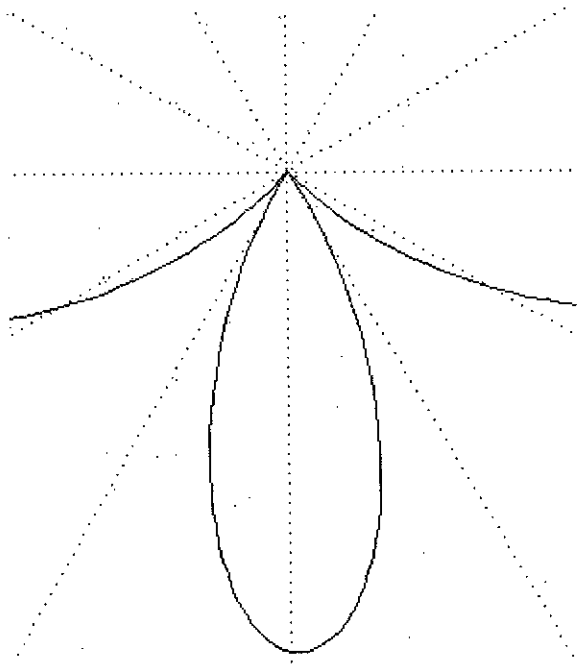


Fig. 5.6 Magnified rear view of the H-plane pattern of the Yagi-Uda array

## 5.4 Discussion

Comparison between azimuthal far-field radiation patterns of different antennas is given in the following figure.

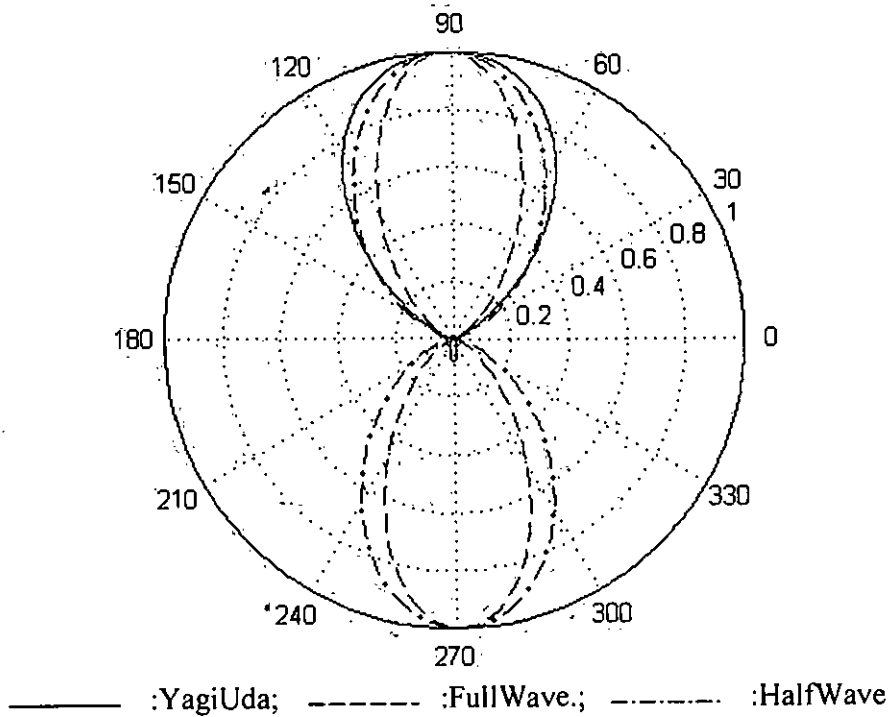


Fig. 5.7 Comparison for azimuthal pattern of the half-wave, full-wave and Yagi-Uda array

From the figure 5.7, it is found that the radiation pattern of the full-wave dipole is narrower than that of half-wave dipole. It represents that the full-wave dipole is more directive than the half-wave dipole antenna. Comparing the radiation pattern of a dipole antenna with that of a Yagi-Uda array we can say that the Yagi-Uda array can be used to direct radiated power towards a desired angular sector. The radiation pattern of Yagi-Uda array has only one lobe, when both the full-wave and half-wave dipole has symmetrical two lobes. The most basic property of the array is that, the relative displacements of the antenna elements with respect to each other introduce relative phase shifts in the radiation vectors, which can then add constructively in some directions or destructively in others. Radiation pattern for receiving antenna has not been calculated here, considering the reciprocity property.

**CHAPTER - 6**  
**GENERAL DISCUSSION**

## 6.1 General Discussion

The current distributions for a half-wave, a full-wave dipole antenna and a three-element Yagi-Uda antenna array have been calculated by solving Pocklington's integral equation using wavelet bases in moment method. The calculation has been followed at different scales to select the appropriate scale for analysis. From the results it is found that – for analysis of half-wave dipole current distribution, scale equals to three is the most efficient considering the computation time and information detail of the calculated current distribution. Similarly, for full-wave dipole, the analysis is most efficient at fourth scale with respect to the calculation time and shape of the current function. Determined current distributions at efficient scale have been compared with theoretical and experimental data. The accuracy level is comparatively acceptable, even at the lowest scale. For the three-element Yagi-Uda array, the computation time is higher. Current distributions on each antenna element have been calculated and also verified with the theoretical values based on King's Three-term approximation for a ten-element array. The results are found acceptable in most cases. From the corresponding current distribution, two basic antenna properties, i.e. antenna input impedance and far-field radiation pattern have been determined. In most cases, the analyzed antenna input impedances are found very close to the experimental result and theoretical estimation. Calculated far-field radiation patterns are found also physically significant. In the analysis it is noted that - this method is more efficient for electrically small antennas and it takes longer time to analyze the full-wave dipole than half-wave antenna. It demands higher computation power as antenna length increases.

## 6.2 Further Scope of Work

In this method, the computation time is relatively higher (43 to 107 times) than the time required in case of Numerical Electromagnetic Code (NEC). NEC is a widely used public domain program for modeling antennas and other structures. NEC solves Pocklington's equation using a spline-like sinusoidal basis and a set of delta functions as weighting functions. In this analysis Galerkin's technique has been followed, i.e. same wavelet bases have been used as both basis and weighting function. Though Galerkin's technique is more complicated from computational perspective, it enforces the boundary condition more rigorously than the point matching technique. However, from the analysis it has been observed that – approximately the total computation time has been used to determine the matrix element. The matrix equation has been solved within a very short time (generally 75 milliseconds). Therefore, to reduce the computation time significantly, more efficient method should be implemented to evaluate the matrix element. Quadrature methods (e.g. Gauss-Legendre, Gauss-Kronrod etc.) should be implemented more efficiently to reduce the computation time to the NEC level.

## APPENDIX – A.1 Physical Constants

Quantity	Symbol	Value	Unit
Speed of light in free space	$c$	299 792 458	$\text{ms}^{-1}$
Permittivity of free space	$\epsilon_0$	$8.854\ 187\ 817 \times 10^{-12}$	$\text{F m}^{-1}$
Permeability of free space	$\mu_0$	$4\pi \times 10^{-7}$	$\text{H m}^{-1}$
Characteristic impedance of free space	$\eta$	376.730 313 461	$\Omega$
Propagation constant in free space	$k_0$	$2\pi/\lambda_0$	$\text{rad m}^{-1}$
Electron charge	$e$	$1.602\ 176\ 462 \times 10^{-19}$	C
Electron mass	$m_e$	$9.109\ 381\ 887 \times 10^{-31}$	kg

## APPENDIX – A.2 Relative Error

The relative error of  $f_r$  with respect  $f_0$  is defined by –

$$\begin{aligned} \epsilon_{f_0 f_r} &= \frac{\|f_0 - f_r\|_2}{\|f_0\|_2} \times 100\% \\ &= \frac{\sqrt{\frac{1}{N} \left[ \sum_{n=1}^{n=N} (f_0 - f_r)^2 \right]}}{\sqrt{\frac{1}{N} \sum_{n=1}^{n=N} f_0^2}} \times 100\% \end{aligned}$$

$$\epsilon_{WM} = \frac{\|f_{Mack} - f_{Wavelets}\|_2}{\|f_{Mack}\|_2} \times 100\%$$

$$\epsilon_{WK} = \frac{\|f_{King} - f_{Wavelets}\|_2}{\|f_{King}\|_2} \times 100\%$$

$$\epsilon_{KM} = \frac{\|f_{Mack} - f_{King}\|_2}{\|f_{Mack}\|_2} \times 100\%$$

## APPENDIX – B. Computer Programs

### List of Routines

Routine	Function
function_Tx.m	To determine the current distribution of a transmitting antenna
function_Rx.m	To determine the current distribution of a receiving antenna
function_Yagi_Uda.m	To determine the current distribution of each antenna of a Yagi-Uda array
find_scale.m	Sub-routine to find scale
find_k.m	Sub-routine to find k-value
scale_cof.m	Sub-routine to determine scale function co-efficient
scalef.m	Sub-routine to construct scale function
wavelet_cof.m	Sub-routine to determine wavelet function co-efficient
wavelet.m	Sub-routine to construct wavelet function
basef.m	Sub-routine to determine the matrix elements
krnl1.m	Sub-routine to calculate the kernel value
TwoD.m	Sub-routine for quadrature (Copyright 2008 : Lawrence F. Shampine)
plot_Iz.m	Sub-routine to plot antenna current distribution

In the thesis, to calculate the current distribution of the wire antenna, following resources have been used –

Programming Software : Matlab 7.6.0 (R2008a)  
CPU Clock Speed : Celeron 1.7 GHz  
RAM Capacity : 256 MB

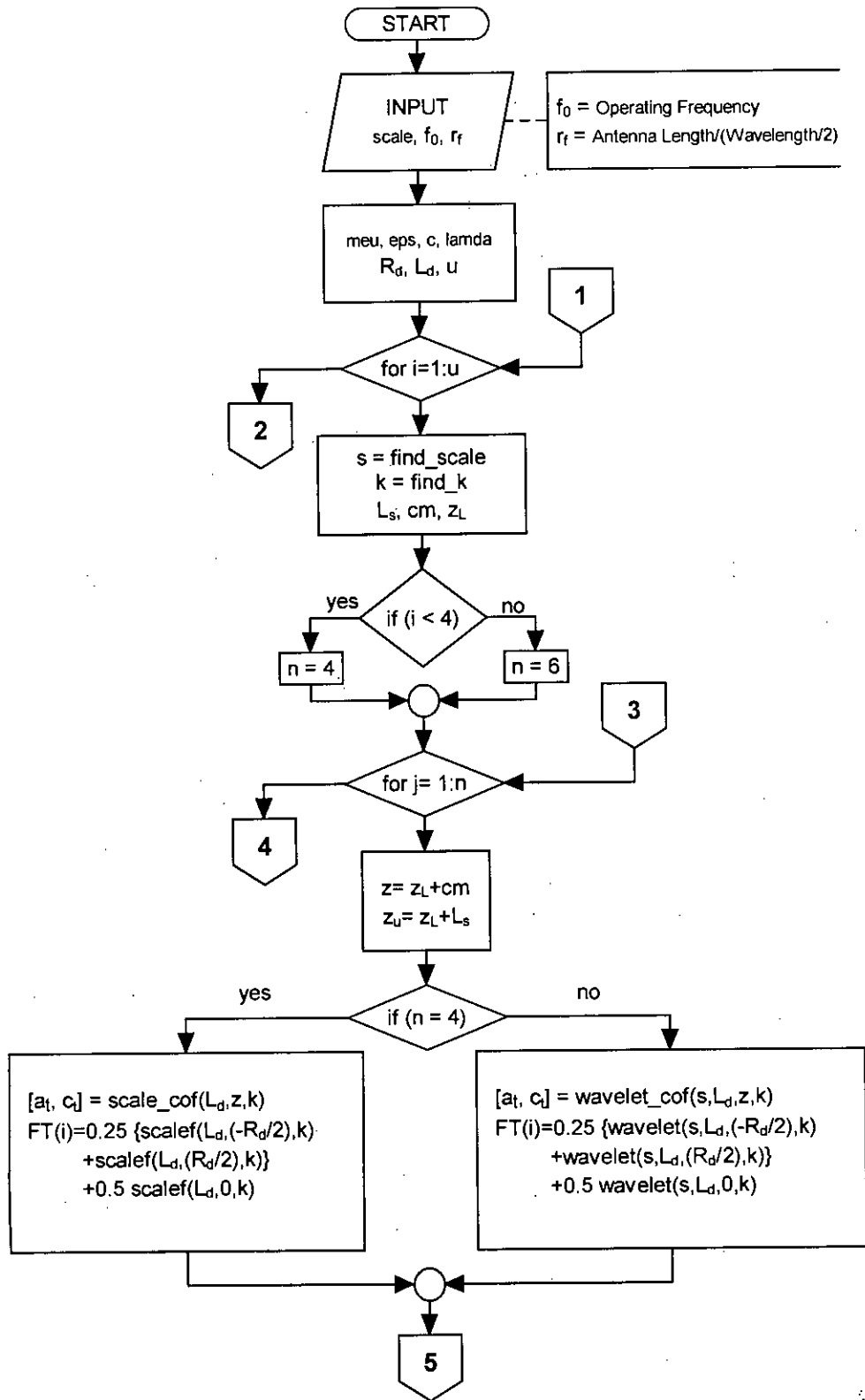


Fig.B.1 Flow Chart to calculate Current Distribution of Wire Antenna (Start)

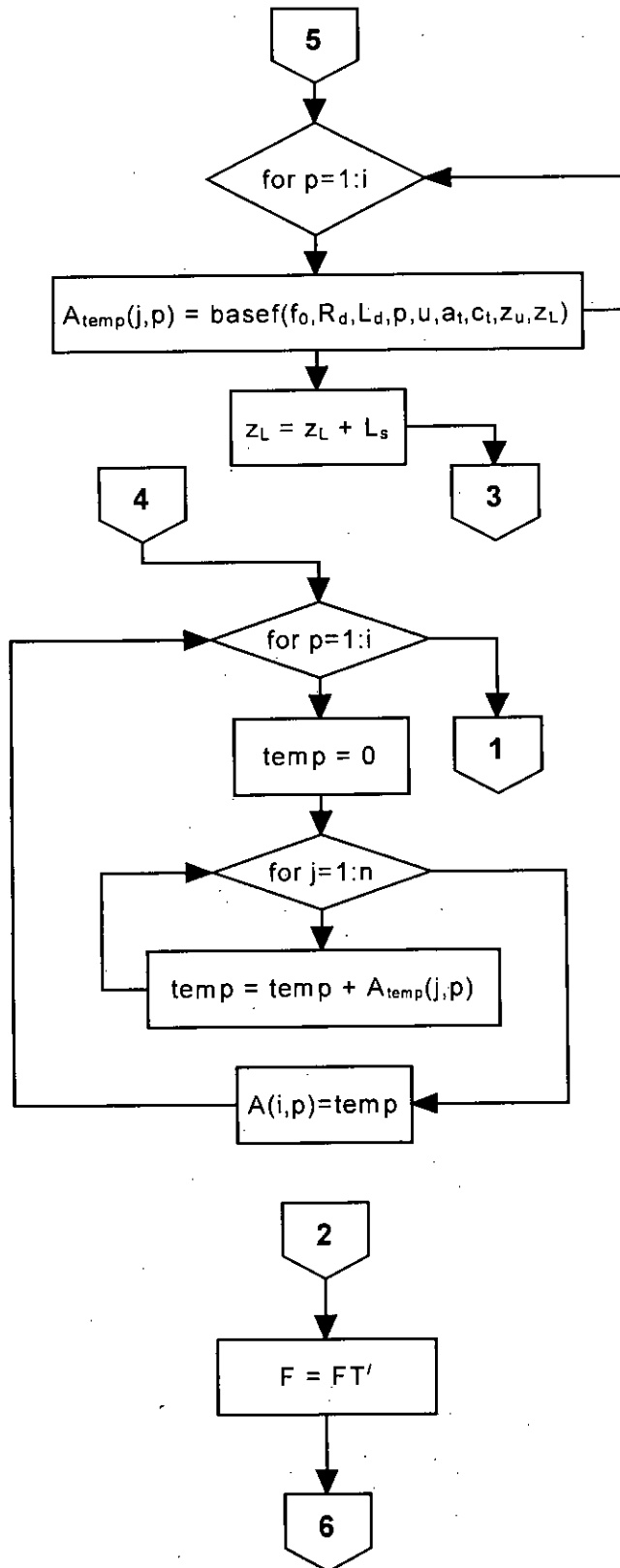


Fig.B.2 Flow Chart to calculate Current Distribution (Continued...)



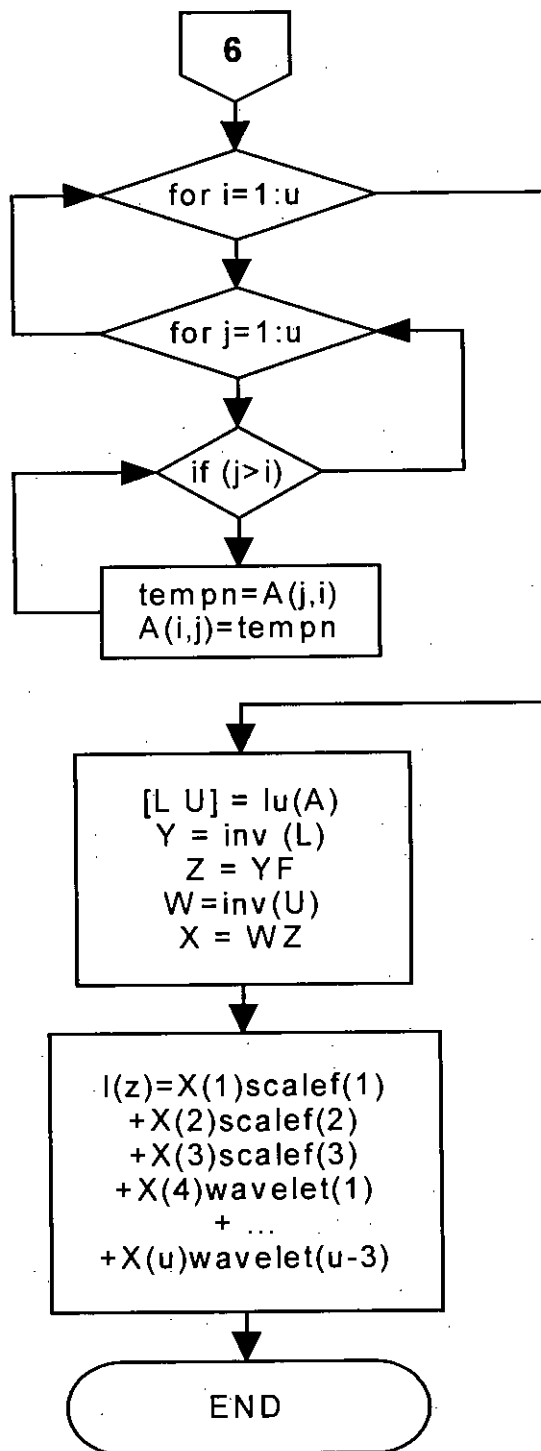


Fig.B.3 Flow Chart to calculate Current Distribution (End)

```

*****
% Function for I(z) of a center-feed delta gap transmitting antenna %
*****

```

```

%Inputs
scale=3;           %Scale of analysis
f0=3e8;           %Operating frequency in Hertz
rf=1;             %Antenna Length/Half-wavelength ratio

tic;

meu=(4e-7)*pi;    %Permeability of space (H/m)
eps=8.854e-12;    %Permittivity of space (F/m)
c=1/(sqrt(meu*eps)); %Velocity of the wave in space (m/s)
lamda=c/f0;       %Wavelength

Rd=(7.022e-3)*lamda; %Radius of cylindrical linear antenna
Ld=(rf*lamda)/2;    %Length of cylindrical linear antenna

u=3;
for i=2:scale
    u=u+(2^i)-2;
end

Atemp=zeros(6,u);
A=zeros(u,u);
FT=zeros(1,u);

for i=1:u
    s=find_scale(i,u);
    k=find_k(i,u);

    Ls=Ld/(2^(s+1));
    cm=Ls/2;
    zL=((k*Ld)/(2^s))-(Ld/2);

    if(i<4)
        n=4;
    else
        n=6;
    end

    for j=1:n
        z=zL+cm;
        zu=zL+Ls;

        if(n==4)
            [at,ct]=scale_cof(Ld,z,k);
            FT(i)=0.25*(scalef(Ld,(-Rd/2),k)+scalef(Ld,(Rd/2),k))...
                +0.5*scalef(Ld,0,k); %Calculated for V0=1Volt and delz=Rd
        else
            [at,ct]=wavelet_cof(s,Ld,z,k);
            FT(i)=0.25*(wavelet(s,Ld,(-Rd/2),k)+...

```

```

        wavelet(s,Ld,(Rd/2),k))+0.5*wavelet(s,Ld,0,k);
    %Calculated for V0=1Volt and delz=Rd

    end

    for p=1:i
        Atemp(j,p)=basef(f0,Rd,Ld,p,u,at,ct,zu; zL);
    end

    zL=zL+Ls;
end

for p=1:i
    temp=0;
    for j=1:n
        temp=temp+Atemp(j,p);
    end
    A(i,p)=temp;
end
end

F=FT';

for i=1:u
    for j=1:u
        if(j>i)
            tempn=A(j,i);
            A(i,j)=tempn;
        end
    end
end

[L U]=lu(A);
Y=inv(L);
Z=Y*F;
W=inv(U);
X=W*Z;

pf=plot_Iz(f0,rf,s,X); %Plot function to plot current distribution

toc;

```

```

%%%%%%%%%%%%%%%%%%%%%%%%%%%%%%%%%%%%%%%%%%%%%%%%%%%%%%%%%%%%%%%%%%%%%%%%
% Function for I(z) of a uniform plane-wave receiving antenna %
%%%%%%%%%%%%%%%%%%%%%%%%%%%%%%%%%%%%%%%%%%%%%%%%%%%%%%%%%%%%%%%%%%%%%%%%

```

```

%Inputs
scale=3;           %Scale of analysis
f0=3e8;           %Operating frequency in Hertz
rf=1;             %Antenna Length/Half-wavelength ratio

tic;

meu=(4e-7)*pi;    %Permeability of space (H/m)
eps=8.854e-12;    %Permittivity of space (F/m)
c=1/(sqrt(meu*eps)); %Velocity of the wave in space (m/s)
lamda=c/f0;       %Wavelength

Rd=(7.022e-3)*lamda; %Radius of cylindrical linear antenna
Ld=(rf*lamda)/2;    %Length of cylindrical linear antenna

u=3;
for i=2:scale
    u=u+(2^i)-2;
end

Atemp=zeros(6,u);
A=zeros(u,u);
FT=zeros(1,u);

for i=1:u
    s=find_scale(i,u);
    k=find_k(i,u);

    Ls=Ld/(2^(s+1));
    cm=Ls/2;
    zL=((k*Ld)/(2^s))-(Ld/2);

    if(i<4)
        n=4;
    else
        n=6;
    end

    ftemp=0;
    for j=1:n
        z=zL+cm;
        zu=zL+Ls;

        if(n==4)
            [at,ct]=scale_cof(Ld,z,k);
            ftemp=ftemp+0.5*(zu-zL)*(scalef(Ld, zu, k)+scalef(Ld, zL, k));
        else
            [at,ct]=wavelet_cof(s,Ld,z,k);
            ftemp=ftemp+0.5*(zu-zL)*(wavelet(s,Ld, zu, k)+...

```

```

        wavelet(s, Ld, zL, k));

    end

    for p=1:i
        Atemp(j, p)=basef(f0, Rd, Ld, p, u, at, ct, zu, zL);
    end

    zL=zL+Ls;
end

FT(i)=ftemp;

for p=1:i
    temp=0;
    for j=1:n
        temp=temp+Atemp(j, p);
    end
    A(i, p)=temp;
end
end

F=FT';

for i=1:u
    for j=1:u
        if(j>i)
            tempn=A(j, i);
            A(i, j)=tempn;
        end
    end
end

[L U]=lu(A);
Y=inv(L);
Z=Y*F;
W=inv(U);
X=W*Z;

pf=plot_Iz(f0, rf, s, X); %Plot function to plot current distribution

toc;

```

```

%%%%%%%%%%%%%%%%%%%%%%%%%%%%%%%%%%%%%%%%%%%%%%%%%%%%%%%%%%%%%%%%%%%%%%%%
% Function for I(z) on each antenna of a 3-element Yagi-Uda array %
%%%%%%%%%%%%%%%%%%%%%%%%%%%%%%%%%%%%%%%%%%%%%%%%%%%%%%%%%%%%%%%%%%%%%%%%

```

```

%Inputs
scale=3; %Scale of analysis
f0=3e8; %Operating frequency in Hertz
ryr=0.51; %Antenna Length/Wavelength ratio for reflector
rya=0.5; %Antenna Length/Wavelength ratio for active
dipole
ryd=0.4; %Antenna Length/Wavelength ratio for director

tic;

meu=(4e-7)*pi; %Permeability of space (H/m)
eps=8.854e-12; %Permittivity of space (F/m)
c=1/(sqrt(meu*eps)); %Velocity of the wave in space (m/s)
lamda=c/f0; %Wavelength

Rd=(3.37e-3)*lamda; %Radius of cylindrical linear antenna
na=3; %Total number of antenna element
Lr=ryr*lamda; %Length of reflector antenna
La=rya*lamda; %Length of active antenna element
Ld=ryd*lamda; %Length of director antenna
dar=0.25*lamda; %Spacing between reflector and active antenna
dad=0.3*lamda; %Spacing between director and active antenna
drd=dar+(na-2)*dad; %Spacing between reflector and director antenna

u=3;
for i=2:scale
    u=u+(2^i)-2;
end

A=zeros(na*u,na*u);
F=zeros(na*u,1);
Atemp=zeros(6,u);
Ac=zeros(u,u);
FT=zeros(1,u);

for v=1:na
    if(v==1)
        Lt=Lr;
    elseif(v==2)
        Lt=La;
    else
        Lt=Ld;
    end

    for w=1:na
        if(w==1)
            Lb=Lr;
        elseif(w==2)
            Lb=La;
        else

```

```

    Lb=Ld;
end

if(w==v)
    a=Rd;
elseif ((v==1)&&(w==2))||((v==2)&&(w==1))
    a=dar;
elseif ((v==1)&&(w==3))||((v==3)&&(w==1))
    a=drd;
else
    a=dad;
end

%%% Core for Analysis (START) %%%
for i=1:u
    s=find_scale(i,u);
    k=find_k(i,u);

    Ls=Lt/(2^(s+1));
    cm=Ls/2;
    zL=((k*Lt)/(2^s))-(Lt/2);

    if(i<4)
        n=4;
    else
        n=6;
    end

    for j=1:n
        z=zL+cm;
        zu=zL+Ls;

        if(n==4)
            [at,ct]=scale_cof(Lt,z,k);
            if((w==2)&&(v==2))
                FT(i)=0.25*(scalef(Lt,(-Rd/2),k)+...
                    scalef(Lt,(Rd/2),k))+0.5*scalef(Lt,0,k);
                %Calculated for V0=1Volt and delz=Rd
            end
        else
            [at,ct]=wavelet_cof(s,Lt,z,k);
            if((w==2)&&(v==2))
                FT(i)=0.25*(wavelet(s,Lt,(-Rd/2),k)+...
                    wavelet(s,Lt,(Rd/2),k))+...
                    +0.5*wavelet(s,Lt,0,k);
                %Calculated for V0=1Volt and delz=Rd
            end
        end
    end

    if(w==v)
        tp=i;
    else
        tp=u;
    end
end

```

```

        for p=1:tp
            Atemp(j,p)=basef(f0,a,Lb,p,u,at,ct,zu,zL);
        end

        zL=zL+Ls;
    end

    for p=1:tp
        temp=0;
        for j=1:n
            temp=temp+Atemp(j,p);
        end
        Ac(i,p)=temp;
    end

end

if(w==v)
    for i=1:u
        for j=1:u
            if(j>i)
                tempn=Ac(j,i);
                Ac(i,j)=tempn;
            end
        end
    end
end

%%% Core for Analysis (END) %%%

rs=(v-1)*u+1;
re=v*u;
cs=(w-1)*u+1;
ce=w*u;

e=1;
for q=rs:re
    g=1;
    for t=cs:ce
        A(q,t)=Ac(e,g);
        g=g+1;
    end
    if((w==2)&&(v==2))
        F(q)=FT(e);
    end
    e=e+1;
end

end

end

%%% Final Calculation (START) %%%
[L U]=lu(A);
Y=inv(L);
Z=Y*F;

```



```

W=inv(U);
X=W*Z;
%%% Final Calculation (END) %%%

Xr=X(1:u);
Xa=X((u+1):(2*u));
Xd=X(((2*u)+1):(3*u));

figure; pfr=plot_Iz(f0,ryr,scale,Xr);
figure; pfa=plot_Iz(f0,rya,scale,Xa);
figure; pfd=plot_Iz(f0,ryd,scale,Xd);

toc;

```

```

%%%%%%%%%%%%%%%%%%%%%%%%%%%%%%%%%%%%%%%%%%%%%%%%%%%%%%%%%%%%%%%%%%%%%%%%
% Function to determine the scale of scale or wavelet functions %
%%%%%%%%%%%%%%%%%%%%%%%%%%%%%%%%%%%%%%%%%%%%%%%%%%%%%%%%%%%%%%%%%%%%%%%%

```

```

function[scale]=find_scale(x,u)
% x= Loop variable
% u= Total number of variable or matrix element

sLim=3;
for sL=2:u
    sLim=(2^sL)-2+sLim;
    if(x<=sLim)
        scale=sL;
        return;
    end
end

```

```

%%%%%%%%%%%%%%%%%%%%%%%%%%%%%%%%%%%%%%%%%%%%%%%%%%%%%%%%%%%%%%%%%%%%%%%%
% Function to find the value of k of scale or wavelet functions %
%%%%%%%%%%%%%%%%%%%%%%%%%%%%%%%%%%%%%%%%%%%%%%%%%%%%%%%%%%%%%%%%%%%%%%%%

```

```

function[k]=find_k(x,u)
% x= Loop variable
% u= Total number of variable or matrix element

if(x<4)
    k=x-1;
else
    s=find_scale(x,u);
    sLim=3;
    for sL=2:(s-1)
        sLim=sLim+((2^sL)-2);
    end
    k=(x-1)-sLim;
end

```

```
*****
% Function to determine co-efficient of scale function at scale =2 %
*****
```

```
function[a,c]=scale_cof(L,z,k)
% L= Length of the antenna
% z= z-value
% k= k-value of the scale function
```

```
zj=(4/L)*(z+(L/2));
if((zj>=k)&&(zj<=(k+1)))
    a=4/L;
    c=2-k;
elseif((zj>=(k+1))&&(zj<=(k+2)))
    a=-4/L;
    c=k;
else
    a=0;
    c=0;
end
```

```
*****
% Scale Function at scale=2 %
*****
```

```
function[out]=scalef(L,z,k)
% L= Length of the antenna
% z= z-value
% k= k-value of scale function
```

```
zj=(4/L)*(z+(L/2));
if((zj>=k)&&(zj<=(k+1)))
    out=zj-k;
elseif((zj>=(k+1))&&(zj<=(k+2)))
    out=2-(zj-k);
else
    out=0;
end
```

```

*****
% Function to determine co-efficient of wavelet function %
*****

```

```

function[a,c]=wavelet_cof(j,L,z,k)
% j= scale of the wavelet function
% L= Length of the antenna
% z= z-value
% k= k-value of the wavelet function

```

```

cw=0.166667;
J=2^j;
J1=2^(j-1);
zj=(J/L)*(z+(L/2));
if((zj>=k)&&(zj<=(k+.5)))
    a=(cw*J)/L;
    c=cw*(J1-k);
elseif((zj>=(k+.5))&&(zj<=(k+1)))
    a=-(7*cw*J)/L;
    c=cw*((7*k)-(7*J1)+4);
elseif((zj>=(k+1))&&(zj<=(k+1.5)))
    a=(16*cw*J)/L;
    c=cw*((16*J1)-(16*k)-19);
elseif((zj>=(k+1.5))&&(zj<=(k+2)))
    a=-(16*cw*J)/L;
    c=cw*((16*k)-(16*J1)+29);
elseif((zj>=(k+2))&&(zj<=(k+2.5)))
    a=(7*cw*J)/L;
    c=cw*((7*J1)-(7*k)-17);
elseif((zj>=(k+2.5))&&(zj<=(k+3)))
    a=-(cw*J)/L;
    c=cw*(k-J1+3);
else
    a=0;
    c=0;
end

```

```

*****
% Wavelet Function %
*****

```

```

function[wv]=wavelet(j,L,z,k)
% j= scale of the wavelet function
% L= Length of the antenna
% z= z-value
% k= k-value of the wavelet function

```

```

c=0.166667;
J=2^j;
zj=(J/L)*(z+(L/2));
if((zj>=k)&&(zj<=(k+.5)))
    wv=c*(zj-k);

```

```

elseif((zj>=(k+.5))&&(zj<=(k+1)))
    wv=c*(4-7*(zj-k));
elseif((zj>=(k+1))&&(zj<=(k+1.5)))
    wv=c*(-19+16*(zj-k));
elseif((zj>=(k+1.5))&&(zj<=(k+2)))
    wv=c*(29-16*(zj-k));
elseif((zj>=(k+2))&&(zj<=(k+2.5)))
    wv=c*(-17+7*(zj-k));
elseif((zj>=(k+2.5))&&(zj<=(k+3)))
    wv=c*(3-(zj-k));
else
    wv=0;
end

```

```

%%%%%%%%%%%%%%%%%%%%%%%%%%%%%%%%%%%%%%%%%%%%%%%%%%%%%%%%%%%%%%%%%%%%%%%%
% Base function to determine the matrix elements %
%%%%%%%%%%%%%%%%%%%%%%%%%%%%%%%%%%%%%%%%%%%%%%%%%%%%%%%%%%%%%%%%%%%%%%%%

```

```

function[out]=basef(f0,a,L,p,u,at,ct,zu,zL)
% f0= Operating frequency in Hertz
% a= Radius of the wire antenna in meter
% L= Length of the wire antenna in meter
% p= Loop variable
% u= Total number of variable or matrix element
% at= Co-efficient of the testing function
% ct= Constant value of the testing function
% zu= Upper limit of the testing function
% zL= Lower limit of the testing function

meu=(4e-7)*pi;           %Permeability of space (H/m)
eps=8.854e-12;          %Permittivity of space (F/m)
eta=sqrt(meu/eps);       %Intrinsic Impedance
c=1/(sqrt(meu*eps));     %Velocity of the wave in space (m/s)
k0=(2*pi*f0)/c;         %Wave number
lamda=c/f0;

c1=-(3*i*eta*lamda*a*a)/(8*pi*pi);
c2=(3*eta*lamda*k0*a*a)/(8*pi*pi);
c3=(i*eta*lamda*(2+((k0*a)^2)))/(8*pi*pi);
c4=-(eta*lamda*k0)/(4*pi*pi);

s=find_scale(p,u);
k=find_k(p,u);

Ls=L/(2^(s+1));
cm=Ls/2;
zpL=((k*L)/(2^s))-(L/2);
Btemp=0;

if(p<4)
    n=4;
else
    n=6;
end

```

```

for j=1:n
    zp=zl+cm;

    if(n==4)
        [ab,cb]=scale_cof(L,zp,k);
    else
        [ab,cb]=wavelet_cof(s,L,zp,k);
    end

    zpu=zl+Ls;

    krnl = @(x,y)krnl1(x,y,k0,a,ab,at,cb,ct,c1,c2,c3,c4);
    Btemp=Btemp+TwoD(krnl,zL,zu,zpL,zpu);
    zpL=zl+Ls;
end

out=conj(Btemp);

```

```

*****
% Kernel function of each matrix element %
*****

```

```

function z = krnl1(x,y,k0,a,ab,at,cb,ct,c1,c2,c3,c4)
% x,y = z-values of basis and testing function respectively
% k0= Propagation constant in free-space
% a= Radius of the wire antenna in meter
% ab,at= Co-efficients of basis and testing function respectively
% cb,ct= Constants of basis and testing function respectively
% c1,c2,c3,c4= Constants of the kernel

```

```

t = sqrt((x-y).^2 + a*a);
r = exp(-i*k0*t) ./ (t.*t);
P = ((c1./t + c2)./t + c3)./t + c4;
z = (cb*ct*r + r.*(cb*at*x + ab*ct*y + ab*at*x.*y)).*P;

```

```

*****
% Plot function to plot current distribution of linear dipole %
*****

```

```

function[p]=plot_Iz(f0,rf,scale,X)
% f0= Operating frequency in Hertz
% rf= Antenna Length/Half-wavelength ratio for dipole antenna
%   = Antenna Length/Wavelength ratio for Yagi-Uda array element
% scale= Scale of analysis
% X= Co-efficient matrix of I(z)

```

```

meu=(4e-7)*pi;           %Permeability of space (H/m)
eps=8.854e-12;          %Permittivity of space (F/m)
c=1/(sqrt(meu*eps));    %Velocity of the wave in space (m/s)
lamda=c/f0;             %Wavelength

```

```

if(rf<1)
    Ld=rf*lamda;
else
    Ld=(rf*lamda)/2;
end

u=3;
for i=2:scale
    u=u+(2^i)-2;
end

Ls=Ld/(2^(scale+1));
cm=Ls/2;
np=(Ld/cm)+1;
zd=-Ld/2;

I=zeros(np,1);
curl=zeros(np,1);
curi=zeros(np,1);
cura=zeros(np,1);
xp=zeros(np,1);

for j=1:np
    Itemp=0;
    for i=1:u
        if(i<4)
            kp=find_k(i,u);
            sf=scalef(Ld,zd,kp);
            Itemp=Itemp+(sf*X(i));
        else
            sp=find_scale(i,u);
            kp=find_k(i,u);
            wf=wavelet(sp,Ld,zd,kp);
            Itemp=Itemp+(wf*X(i));
        end
    end
    I(j)=Itemp;
    curl(j)=real(I(j));
    curi(j)=imag(I(j));
    cura(j)=abs(I(j));
    xp(j)=zd;
    zd=zd+cm;
end

plot(xp,curl,'-',xp,curi,'--',xp,cura,'-.');
xlabel('Axial Distance (z/lamda)');
ylabel('Normalized Current (Amperes/Volt)');
grid;

p=0;
end

```

105888

## APPENDIX – C Wavelets

Wavelets are building blocks that can be used as the basis of function spaces, i.e. they allow the description of a function in terms of simple elements (or atoms). Such atomic decompositions result in an effective representation of complex data and allow an efficient numerical solution in application. The term ‘wavelets’ is a literal translation of the French word ‘ondelettes’ or ‘petites ondes’, that is, ‘small waves’. This implies that wavelets are waves, namely, functions that are localized in frequency around a central value and that are limited in time.

### The Wavelet Representation

Wavelets are families of functions that integrate to zero and are produced by scaling and translating a single function (called mother wavelet). A wavelet is described by the function  $\psi_{a,b}(t)$  which is obtained by dilation and translation (shift) of a function  $\psi(t)$  as defined by –

$$\psi_{a,b}(t) = \frac{1}{\sqrt{a}} \psi\left(\frac{t-b}{a}\right) \quad (\text{C-1})$$

with  $a > 0$ , and  $b \in \mathfrak{R}$ , where  $\mathfrak{R}$  is the set of real numbers. Dilation of a function  $f(t)$  means  $f(kt)$ ; when  $k$  is some constant.

### Wavelet Transformation

The wavelet transform defined by  $Wf(a,b)$  of a function  $f(t)$  than is expressed as –

$$Wf(a,b) = \int_{-\infty}^{+\infty} f(t) \frac{1}{\sqrt{a}} \psi\left(\frac{t-b}{a}\right) dt \quad (\text{C-2})$$

### Why Use Wavelets?

Wavelets are the function of two parameters, dilation and translation, whereas the Fourier methodology has only dilation. The Fourier technique is a useful tool for analyzing and approximating functions by using an orthonormal set of basis functions, which generally consist of the polynomials of trigonometric functions. In conventional Fourier technique, the normalized functions  $\frac{1}{\sqrt{2\pi}} e^{jm}$  are used, which are dilated version of  $e^{j\omega}$ . Hence,

Fourier series converges in the mean when analyzing functions are periodic. The convergence is point wise if the function is continuous. However, the approximation methodology displays the Gibb’s phenomenon when the Fourier technique is used to approximate a discontinuous function. Gibb’s phenomenon is a problem of overshooting (and undershooting) the approximation to a function by an entire domain basis occurring near the point of discontinuity.

In wavelet analysis – not only an orthonormal set of functions, but also a nonorthogonal linearly independent basis and a collection of linearly dependent functions can be employed. Since wavelets can use discontinuous basis functions, edge effects are reproduced much better in the methodology. Therefore, wavelets can approximate discontinuous functions with a fewer number of functions than Fourier technique.

In addition, to observe a time-varying phenomenon (e.g. the fields radiating from a structure as a function of time), it is required to know the instantaneous bandwidth or effective change in the frequency content as a function of time. Although the time and frequency resolution problem is the result of a physical phenomenon known as 'Heisenberg uncertainty principle' (if a signal is strictly time limited, it can not simultaneously be band limited and vice versa) and exist regardless of the transform used, it is possible to analyze any signal by using wavelet approach of Multi Resolution Analysis (MRA). In MRA the signal is analyzed at different frequencies with different resolutions when every spectral component is resolved equally in the Short Term Fourier Transform (STFT) method.

Wavelets essentially look at the spectrum with a constant  $Q$  window. The parameter  $Q$  is defined as the quality of a signal and is related to the relative bandwidth of the wave shape with respect to its center frequency. A constant  $Q$  therefore implies that the ratio of the center frequency with respect to the bandwidth is constant. Thus, when the window is translated to a lower frequency, its support becomes smaller, whereas when the window is moved to a higher frequency region, the window becomes wider, so that the ratio remains the same. Therefore, the bandwidth of the window is a function of the center frequency of observation for a wavelet, whereas for Fourier techniques the observation window is the same irrespective of the center frequency of the observation. This is a serious limitation of the Fourier technique because it is not practical to observe the variations in the spectrum of a waveform.

MRA is designed to give good time resolution and poor frequency resolution at high frequencies and good frequency resolution and poor time resolution at low frequencies. This approach makes sense especially when the signal at hand has high frequency components for short durations and low frequency components for long durations. Fortunately, the signals that are encountered in practical applications are often of this type.

### **B-spline Wavelets**

So far we talked about general wavelet functions. When we select a family of wavelets it is necessary to take into account the properties of this particular family which may have impact on the intended application.

Some important properties of the wavelet function are –

1. Orthogonality
2. Support and Decay



3. Regularity: smooth basis functions are desired in applications where derivative are involved.
4. Vanishing Moments
5. Symmetry: is desirable because makes it easier to deal with boundary conditions.

The B-spline wavelets have all the desirable properties listed above.

### **The Scale**

The parameter **scale** in the wavelet analysis is similar to the scale used in maps. As in the case of maps, high scales correspond to a non-detailed global view and low scales correspond to a detailed view. Similarly, in terms of frequency, low frequencies (high scales) correspond to a global information of a signal (that usually spans the entire signal), whereas high frequencies (low scales) correspond to a detailed information of a hidden pattern in the signal (that usually lasts a relatively short time).

Scaling, as a mathematical operation, either dilates or compresses a signal. Larger scales correspond to dilated (or stretched out) signals and small scales correspond to compressed signals. In terms of mathematical functions, if  $f(t)$  is a given function  $f(st)$  corresponds to a contracted (compressed) version of  $f(t)$  if  $s > 1$  and to an expanded (dilated) version of  $f(t)$  if  $s < 1$ . However, in the definition of the wavelet transform, the scaling term is used in the denominator, and therefore, the opposite of the above statements is true, i.e., higher scales correspond to detailed information of the function whereas lower scales correspond to non-detailed information of the function.

## APPENDIX – D Moment Method

The integral equations are solved numerically by the method of moments. The basic procedure for this solution is described in this section.

### Outline of the Moment Method

The method of moments applies to a general linear-operator equation,

$$L f = e \quad (\text{D-1})$$

where  $e$  is a known excitation,  $f$  is an unknown response and  $L$  is a linear operator (an integral operator in the present case). The unknown function  $f$  is expanded in a sum of basis functions  $f_i$  as –

$$f = \sum_{j=1}^N \alpha_j f_j \quad (\text{D-2})$$

and a set of linear equations for the coefficients  $\alpha_j$  is then obtained by taking the inner product of equation  $L f = e$  with a set of weighting functions  $w_i$  as –

$$\langle w_i, L f \rangle = \langle w_i, e \rangle \text{ where, } i = 1, \dots, N. \quad (\text{D-3})$$

The inner product is typically defined as –

$$\langle f, g \rangle = \int_S f(r) g(r) dA \quad (\text{D-4})$$

where the integration is over the structure surface. The number of weighting functions is taken here to be equal to the number of basis functions, so that the number of equations is equal to the number of unknown coefficients in  $f$ . Due to the linearity of  $L$ , substitution of  $f$  yields –

$$\sum_{j=1}^N \alpha_j \langle w_i, L f_j \rangle = \langle w_i, e \rangle \text{ where, } i = 1, \dots, N. \quad (\text{D-5})$$

This set of linear equations can be written in matrix notation as –

$$[G] [A] = [E] \quad (\text{D-6})$$

where,  $G_{ij} = \langle w_i, L f_j \rangle$ ,  $A_j = \alpha_j$  and  $E_i = \langle w_i, e \rangle$ . The solution can then be written in terms of the inverse matrix as –

$$[A] = [G]^{-1} [E] \quad (\text{D-7})$$

The choice of basis and weighting functions has an important role in determining the efficiency and accuracy of the moment-method solution. Each basis function can either extend over the entire domain of the current, or a sub-domain. Common choices for the basis functions are rectangular pulses, piecewise-linear or piecewise-sinusoidal functions, or polynomials. When  $w_i = f_i$ , the procedure is known as Galerkin's technique.

## APPENDIX – E Gauss Quadrature

In numerical analysis, a quadrature rule is an approximation of the definite integral of a function, usually stated as a weighted sum of function values at specified points within the domain of integration. An  $n$ -point Gaussian quadrature rule, named after Carl Friedrich Gauss, is a quadrature rule constructed to yield an exact result for polynomials of degree  $2n - 1$  or less by a suitable choice of the points  $x_i$  and weights  $w_i$  for  $i = 1, \dots, n$ . The domain of integration for such a rule is conventionally taken as  $[-1, 1]$ , so the rule is stated as –

$$\int_{-1}^1 f(x) dx \approx \sum_{i=1}^n w_i f(x_i) \quad (\text{E-1})$$

### Change of interval for Gaussian quadrature

An integral over  $[a, b]$  must be changed into an integral over  $[-1, 1]$  before applying the Gaussian quadrature rule. This change of interval can be done in the following way –

$$\int_a^b f(x) dx = \frac{b-a}{2} \int_{-1}^1 f\left(\frac{b-a}{2}x + \frac{a+b}{2}\right) dx \quad (\text{E-2})$$

After applying the Gaussian quadrature rule, the following approximation is obtained –

$$\int_a^b f(x) dx = \frac{b-a}{2} \sum_{i=1}^n w_i f\left(\frac{b-a}{2}x_i + \frac{a+b}{2}\right) \quad (\text{E-3})$$

### Other forms of Gaussian quadrature

The integration problem can be expressed in a slightly more general way by introducing a positive weight function  $\omega$  into the integrand, and allowing an interval other than  $[-1, 1]$ .

That is, the problem is to calculate  $-\int_a^b \omega(x) f(x) dx$ , for some choices of  $a$ ,  $b$ , and  $\omega$ .

For  $a = -1$ ,  $b = 1$ , and  $\omega(x) = 1$ , the problem is the same as that considered above and the adaptive method is known as Gauss-Legendre quadrature.

### Gauss-Kronrod Quadrature

An adaptive Gaussian quadrature method for numerical integration in which error is estimation based on evaluation at special points known as "Kronrod points." By suitably picking these points, abscissas from previous iterations can be reused as part of the new set of points, whereas usual Gaussian quadrature would require re-computation of all abscissas at each iteration. This is particularly important when some specified degree of accuracy is needed but the number of points needed to achieve this accuracy is not known ahead of time. Kronrod (1964) showed how to pick Kronrod points optimally from Legendre-Gauss quadrature, and Patterson (1968, 1969) showed how to compute continued extensions of this kind.

## APPENDIX – F LU Factorization

For any nonsingular matrix  $[A]$  on which one can conduct Naïve Gauss Elimination forward elimination steps, one can always write it as –

$$[A] = [L] [U] \quad (\text{F-1})$$

where,  $[L]$  = Lower triangular matrix  
 $[U]$  = Upper triangular matrix

Then if one is solving a set of equations –

$$[A] [X] = [C] \quad (\text{F-2})$$

then,

$$[L] [U] [X] = [C] \quad (\text{F-3})$$

$$[L]^{-1} [L] [U] [X] = [L]^{-1} [C] \quad (\text{F-4})$$

$$[I] [U] [X] = [L]^{-1} [C] \quad (\text{F-5})$$

$$[U] [X] = [L]^{-1} [C] \quad (\text{F-6})$$

Let,  $[L]^{-1} [C] = [Z]$  then  $[L] [Z] = [C]$  and  $[U] [X] = [Z]$ . So we can solve  $[L]^{-1} [C]$  first for  $[Z]$  and then use  $[U]^{-1} [Z]$  to calculate  $[X]$ .

Without proof, the computational time required to decompose the  $[A]$  matrix to  $[L] [U]$  form is proportional to  $n^3/3$ , where  $n$  is the number of equations (size of  $[A]$  matrix). Then to solve the  $[L] [Z] = [C]$ , the computational time is proportional to  $n^2/2$ . Then to solve the  $[U] [X] = [Z]$ , the computational time is proportional to  $n^2/2$ . So the total computational time to solve a set of equations by LU decomposition is proportional to  $(n^3/3) + n^2$ . The total computational time required to find the inverse of a matrix using LU decomposition is proportional to  $(n^3/3) + n(n^2) = (4n^3/3)$ .

**Decomposing  $[A] = [L] [U]$ :**

1. The elements of the  $[U]$  matrix are exactly the same as the coefficient matrix one obtains at the end of the forward elimination steps in Naïve Gauss Elimination.
2. The lower triangular matrix  $[L]$  has 1 in its diagonal entries. The non-zero elements on the non-diagonal elements in  $[L]$  are multipliers that made the corresponding entries zero in the upper triangular matrix  $[U]$  during forward elimination.

## REFERENCES

- [1] Stutzman, W.L. and Thiele, G.A., "Antenna Theory and Design," John Willey & Sons, Inc., 1998.
- [2] Maxwell J. C., "A Dynamical Theory of the Electromagnetic Field," in Proc. Royal Soc. (London), vol. 13, pp. 531, 1864.
- [3] Hertz H., "Ueber Sehr Schnelle Electriche Schwingungen," Wied. Ann., vol. 31, pp. 421, 1887.
- [4] Pocklington H.C., "Electrical Oscillations in Wires," in Proc. Camb. Phil. Soc. 9, pp. 324-333, 25 October 1897.
- [5] Lorenz L., "On the Identity of the Vibrations of Light with Electrical Currents", Phil. Mag. 34, pp. 287-301, June 1867.
- [6] Carter P. S., "Circuit Relations in Radiating Systems and Applications to Antenna Problems," in Proc. IRE, vol. 20, pp. 1004-1041, June 1932.
- [7] Brown G. H., "Directional Antennas," in Proc. IRE, vol. 25, pp. 79-145, January 1937.
- [8] King L.V., "On the Radiation Field of a Perfectly Conducting Base-insulated Cylindrical Antenna over a Perfectly Conducting Plane Earth and the Calculation of Radiation Resistance and Reactance," Phil. Trans. Roy. Soc. (London), ser. A, vol. 236, pp. 381-422, 2 November 1937.
- [9] Hallén E., "Theoretical Investigations into the Transmitting and Receiving Antennae," Nova Acta Regiae Soc. Sci. Upsaliensis, Ser. 4, vol. 2, p. 1, November 1938.
- [10] King Ronald W. P. and Wu Tai Tsun, "Currents, Charges and Near Fields of Cylindrical Antennas," Radio Science Journal of Research NBS/UNSC-URSI, vol. 69D, No. 3, pp. 429-446, March 1965.
- [11] King R. and Middleton D., "The Cylindrical Antenna: Current and Impedance," Quart. Appl. Math, vol. 3, pp. 302-335, 1946.
- [12] Duncan R. H. and Hinchey F., "Cylindrical Antenna Theory," J. Res. NBS, vol. 64D, pp. 569-584, September-October 1960.
- [13] Harrington R. F., "Matrix Methods for Field Problems," in Proc. IEEE, vol. 55, pp. 136-149, February 1967.
- [14] Burkholder R. J., "High-frequency Asymptotic Methods for Analyzing the EM Scattering by Open-ended Waveguide Cavities," Ph.D dissertation, The Ohio State University, Columbus, OH, 1989.
- [15] Beylkin G., Coifman R. and Rokhlin V., "Fast Wavelet Transforms and Numerical Algorithms I," Comm. Pure Appl. Math, vol. 44, pp. 141-183, 1991.

- [16] Chui C. K. and Quak E., "Wavelets on a Bounded Interval," in Num. Math. Approx. Theory, D. Braess and L. L. Schumaker, Eds. Basel: Birkhauser Verlag, vol. 9, pp. 53-75, 1992.
- [17] Nevels Robert D., Goswami Jaideva C. & Tehrani Hooman, "Semi-orthogonal Versus Orthogonal Wavelet Basis Sets for Solving Integral Equations," IEEE Transactions on Antennas and Propagation, vol. 45, No. 9, pp. 1332-1339, September 1997.
- [18] Tretiakov Y. and Pan G., "Malvar Wavelet Based Pocklington Equation Solutions to Thin-wire Antennas and Scatterers," Progress In Electromagnetics Research, PIER 47, pp. 123-133, 2004.
- [19] Mack R. B., "A Study of Circular Arrays," Cruft Lab., Harvard University, Cambridge, Mass., Tech. Reports. pp. 381-386, May 1963.
- [20] Patwari A. M. and German John P., "A Study of Coupled Dipole Antennas in Echelon – A Theoretical Solution", The Journal of the Pakistan Engineers, pp. 57-70, February 1969.
- [21] King Ronold W. P., "The Linear Antenna – Eighty Years of Progress", Proceedings of the IEEE, vol. 55, No. 1, pp. 1-16, January 1967.

